

## Interhemispheric synchrony in visual cortex and abnormal postnatal visual experience

Luc Foubert<sup>1</sup>, Daniel Bennequin<sup>2</sup>, Marie-Annick Thomas<sup>1</sup>, Jacques Droulez<sup>1</sup>, Chantal Milleret<sup>1</sup>

<sup>1</sup>Laboratoire de Physiologie de la Perception et de l'Action, Collège-de-France, CNRS UMR 7152, 11 Place Marcelin Berthelot, 75005 Paris, France, <sup>2</sup>Institut de Mathématiques, Université Paris 7 Denis Diderot, UMR CNRS 7586, 2 Place Jussieu, 75005 Paris, France

### TABLE OF CONTENTS

1. Abstract
2. Introduction
3. Materials and methods
  - 3.1. Anatomical study
    - 3.1.1. Experimental groups
    - 3.1.2. Monocular occlusion
    - 3.1.3. Tracer injections, staining method and 3D reconstruction
    - 3.1.4. Axonal morphology
    - 3.1.5. Architecture of individual terminal arbors
  - 3.2. Numerical simulation
    - 3.2.1. Importing anatomical data to Neuron
    - 3.2.2. Model assumptions and procedure
      - 3.2.2.1. The continuous model of Hodgkin and Huxley (HH)
      - 3.2.2.2. Effects of the myelin sheath on spike propagation
      - 3.2.2.3. Transition from saltatory to continuous spike propagation
      - 3.2.2.4. Implementation of the model on the diverse real morphologies of callosal axons
4. Results
  - 4.1. Anatomical data
    - 4.1.1. Location of the labeled axons in the corpus callosum
    - 4.1.2. Global organization of the MD callosal axons
      - 4.1.2.1. Location of the first node of the MD callosal axons
      - 4.1.2.2. Architecture of the callosal terminal axons
    - 4.1.3. Quantitative analysis of the MD callosal axons
      - 4.1.3.1. Diameters of the trunks of the callosal axons
      - 4.1.3.2. Mean numbers and mean diameters of the 1<sup>st</sup> to the 5<sup>th</sup> order branches of the callosal axons
      - 4.1.3.3. Mean lengths of the 1<sup>st</sup> to the 5<sup>th</sup> order branches of the callosal axons
      - 4.1.3.4. Mean number of nodes of the callosal axons
      - 4.1.3.5. Mean number of terminals of the callosal axons
      - 4.1.3.6. Mean number of boutons of callosal axons
  - 4.2. Simulation of the propagation of spikes in MD callosal axons
5. Discussion
  - 5.1. Effects of monocular occlusion on the morphology of callosal axons
  - 5.2. Simulation of propagation of spikes along the callosal axons
  - 5.3. Possible role of synchronized activities in the development of callosal connections after early monocular deprivation
  - 5.4. Role of synchronized callosal activities during visual processing
6. Acknowledgments
7. References

### 1. ABSTRACT

The question of whether neural synchrony may be preserved in adult mammalian visual cortex despite abnormal postnatal visual experience was investigated by combining anatomical and computational approaches. Single callosal axons in visual cortex of early monocularly deprived (MD) adult cats were labeled anterogradely with biocytin *in vivo* and reconstructed in 3D. Spike propagation was then orthodromically simulated within each of these axons with NEURON® software. Data were systematically compared to those previously obtained in normally reared (NR) adult cats with comparable approaches (1-2). The

architecture of the callosal axons in MD animals differed significantly from the NR group, with longer branches and first nodes located deeper below the cortex. But, surprisingly, simulation of spike propagation demonstrated that transmission latencies of most spikes remained inferior to 2 ms, like the NR group. These results indicate that synchrony of neural activity may be preserved in adult visual cortex despite abnormal postnatal visual experience. According to the temporal binding hypothesis, this also indicates that the necessary timing for visual perception is present despite anatomical abnormalities in visual cortex.

### 2. INTRODUCTION

The “synchrony hypothesis” suggests that neural activities that are spatially separated in mammalian visual cortex may underlie perceptual grouping of visual image features provided they are temporally synchronous (3). Although this temporal binding hypothesis remains controversial (e.g. 4), it is now supported by abundant experimental evidence demonstrating a significant temporal correlation between activities of distant neurons within or between hemispheres. This requires brief propagation times along axons and low variability in arrival times among axon terminals. Such correlations are frequently expressed by a narrow temporal window of phases (within a few milliseconds) for neural oscillatory responses in the gamma band, i.e., in the range of 30-60 Hz (e.g. 5-6-7-8-9-10-11-12; see also 13-14 for reviews). Moreover, the link between gamma band oscillatory activity and visual cognitive tasks has been confirmed in humans (e.g. 15-16). While such temporal correlations have been almost exclusively investigated in normally sighted subjects (see above references), in the present study, the aim was to evaluate whether neural synchrony in adult visual cortex may be preserved despite abnormal postnatal visual experience. This is critical since the anatomy of the neural networks in the visual system, particularly at the cortical level, is generally affected by abnormal viewing conditions. This could lead to asynchrony in the visual neural activity and to altered visual perception. Because it is difficult to investigate function and structure simultaneously at a fine time scale *in vivo*, we combined morphological and computational approaches. The interhemispheric connections *via* the corpus callosum (CC) in cat visual cortex were used as a model. Single visual callosal axons of early monocularly deprived (MD) cats were reconstructed in 3D. The propagation of individual spikes was then simulated in these reconstructed single callosal axons, and the distribution of activation times in their terminals was analyzed and compared to data from normals.

Anatomically, the callosal connections of the normally reared (NR) cat visual cortex display a non-mirror-symmetric organization by linking spatially dispersed sites of each hemisphere that are in visuotopic correspondence (17). Callosal-projecting neurons are distributed rather widely in A17 and A18, by including however the transition zone (TZ) between both areas; by contrast, most of their contralateral terminals are limited to a region that spans the TZ (1-18-19). Functionally, these callosal connections are specifically involved in the neural processing of visual stimuli from along the visual midline and its vicinity, for each of the attributes of objects in the visual scene i.e. orientation, spatial frequency, shape or movement (e.g. 20-21-22-23-24-25). To test the “synchrony hypothesis” at the level of callosal terminals and in order to understand how the geometry of axons is related to propagation of spike activity, Innocenti and collaborators combined anatomical and computational approaches (as we do here) (2). This allowed function and anatomy to be linked at the level of single axons with millisecond precision. They analyzed activation profiles obtained by simulating invasion of an orthodromic action

potential in reconstructed 3D single callosal terminals of axons originating in A17 and A18 of the adult cat. For that, the authors used the *MAXSIM® software*, assuming that callosal axons of NR adult cats are totally myelinated and that the conduction velocity of such axons increases linearly with fiber diameter. In computer simulation, these authors found that conduction from the callosal midline to the first bouton requires latencies of 0.9-3.2 ms, compatible with published electrophysiological values (26-27). They also established that the distribution of activation latencies (i.e. subtracting times of arrivals of the first spike from the last) of the total set of terminal boutons varied across arbors from 0.3 to 2.7 ms. As noted above, such rapid propagation of spike activity, with narrow temporal dispersion of spike arrival times at the terminals of the callosal connections, is a requirement for interhemispheric synchronization of neural activities. Such synchronization was indeed found in numerous studies employing diverse approaches. For example, Engel and collaborators showed that neurons in A17 of cat visual cortex display oscillatory responses that can be synchronized between the hemispheres provided they display similar orientation selectivity, overlapping receptive fields and that the CC is intact (28). By simultaneously recording unit activity in the TZ of each hemisphere of anesthetized and paralyzed cats and by computing cross-correlation histograms between pairs of neurons, Nowak and collaborators also identified the structural basis of cortical synchronization (29). They found three types of cross-correlation histogram peaks, corresponding to three types of temporal coupling characterizing the interhemispheric connections. 1) “T” peak with narrow widths (4-28 ms), 2) “C” peaks with intermediate widths (30-100 ms), and 3) H peaks with large widths (100-1000 ms). More recently, Innocenti and collaborators showed that iso-oriented stimuli presented bilaterally (i.e. in each hemifield) near the visual midline or extending across it causes a significant increase in interhemispheric coherence in the EEG beta-gamma band both in ferrets and in humans (30-31). This was confirmed by analyzing the synchronization of local field potentials recorded through multi-electrodes distributed in the visual cortex of both hemispheres (32). The three latter findings are in agreement with one of our recent studies combining *in vivo* optical imaging of intrinsic signals with labeling of callosal axons which demonstrated that each callosal axon specifically links contralateral cortical regions representing the same orientation and the same location of visual stimuli (33).

After an early abnormal visual experience, the development of callosal connections in cat visual cortex is well known to be greatly altered both anatomically and functionally. This occurs for example after modifying the vision of one eye soon after birth through surgically induced strabismus or monocular deprivation (MD). Both of these manipulations alter the visual cortex in both hemispheres. The visual cortex contralateral to the altered eye is activated through abnormal crossed retino-geniculo-cortical inputs while the visual cortex ipsilateral to the altered eye is activated through abnormal uncrossed retino-geniculo-cortical inputs. In the former, a juvenile-like exuberant distribution of the bodies of the callosal neurons

## Cortical synchrony and abnormal visual experience

is maintained through adulthood whereas they are normally eliminated with age (34). Additionally, in the visual cortex ipsilateral to the altered eye, an abnormally high percentage of cells respond transcallosally suggesting abnormal anatomical properties of the terminals of the callosal neurons (35-36; Milleret *et al.*, in preparation). By contrast, it remains to be determined whether neural synchrony in the adult is preserved in spite of such abnormal conditions of vision early in life. To our knowledge, only one study has approached this question by investigating the effects of early squint on the synchronization of oscillatory responses in cat visual cortex (37). In adult cats reared with divergent squint, the vast majority of cells in A17 became monocularly responsive and only cells activated through a single eye displayed synchronized activities. While great anatomical abnormalities of both intrinsic and inter-areal connections are observed in such animals, anatomy and function have not been linked directly (38).

On the basis of the above described data about callosal connections in early MD cats, the present study first demonstrates that single terminal arbors of callosal axons which have been reconstructed in 3D from the hemisphere ipsilateral to the deprived eye display effectively an abnormal architecture compared to normals, with at least a deeper first node with respect to cortex as well as significantly longer branches. This would have functional implications in light of recent work linking axon branch dynamics and neural activity (e.g. 39-40-41-42-43). Secondly, by simulating the propagation single spikes along these axons using NEURON® software, the present study establishes that almost all evoked spikes in this simulation arrive at the very end of the callosal terminals in a very narrow time window (1-2 ms), as in the NR cats, despite their abnormal architecture. This indicates that rather good intracortical neural synchrony may be preserved despite the morphological changes resulting from an abnormal postnatal visual experience. Interhemispheric synchronization may thus also be preserved. According to the temporal binding hypothesis, this suggests that some aspects of visual perception may occur normally in spite of anatomical abnormalities in visual cortex.

## 3. MATERIALS AND METHODS

In this section, the anterograde labeling of callosal axons from visual cortex of early MD adult cats is described, followed by the methodology for 3D reconstruction of these axons. Then, the simulations for orthodromic spike propagation in each of these axons are detailed.

### 3.1. Anatomical study

Four cats were used in this study (MD9, BMOW1, BMO17 and BMOW2). All surgical procedures conformed to institutional and governmental requirements (Direction of veterinary services and Ethical committee in Paris) and the guidelines of the European Convention for the Protection of Vertebrate Animals Used for Experimental and other Scientific Purposes (Strasbourg, 18.III, 1986).

### 3.1.1. Experimental groups

In the four cats, the eyelids of one eye were sutured shut 6-7 days after birth, i.e. a few days before the natural eye opening (10-12 postnatal days). An anterograde tracer, biocytin, was injected four months later in three animals and five months later for one animal (see below for further details). From their visual cortices, ten callosal axons were reconstructed in 3D. To identify abnormalities, the axonal reconstructions were compared to those obtained from normally-reared (NR) adult cats as previously reported by our team using similar methods (1).

### 3.1.2. Monocular occlusion

In the surgery for monocular lid suture of the young cats, animals were initially anaesthetized with Saffan (10.8 mg/kg of Alfaxalone and 3.6 mg/kg of Alfadolone acetate, Genusxpress, UK; initial, i.m. 1.2 ml/kg, additional, 1:1 in saline, i.v. as required). Temperature was monitored continuously and maintained at 38°C using an electronically controlled heating pad. The eyelids of the *right* eye were sutured after sectioning the limbs being still jointed. A small opening was left as a drain for lachrymal outflow. Two antibiotics (Néomycine and Rifamycine, Chibret) were applied locally as eye drops and a general antibiotic (Extencilline) was finally injected. The first ones were applied both on the day of the surgery and then for one week, while Extencilline was injected only on the day of the surgery.

### 3.1.3. Tracer injections, staining method and 3D reconstruction

Axons were anterogradely filled with pressure-injected biocytin. They were labeled and visualized using procedures described previously for NR adult cats (cf. 1). In brief, biocytin was injected in the *left hemisphere*, i.e., contralateral to the deprived eye (Figure 1). In each injection site, two or three 0.2-0.5 microliters pressure injections separated by ~800 micrometers were achieved in succession through a micropipette, between 500 and 2000 micrometers below the cortical surface. This led to injections including layers I through VI, with diameters ranging between 1400 and 1900 micrometers medio-laterally and 600 and 2300 micrometers antero-posteriorly. In all cases, such sites were wider in supragranular than in infragranular layers. All injections which reached layer VI also labeled axons terminating in the lateral geniculate nucleus, respecting the retinotopic arrangement of the cortico-geniculate connections. Generally, each animal received successive injections in two well separated cortical sites. A first one was performed in the transition zone between areas 17 and 18 (TZ) at Horsley-Clarke stereotaxic coordinates P<sub>2</sub>L<sub>2</sub> or A<sub>9</sub>-L<sub>1.5</sub> (in cats MD9 and BMOW1 respectively; see Figure 1). A second injection was then made more medially within area 17 (A17) at Horsley-Clarke coordinates P<sub>3</sub>L<sub>1</sub> or A<sub>4</sub>L<sub>1</sub> (in cats BMO17 and BMOW2 respectively). Of interest, the latter tracer injections in A17 labeled both “normally” located callosal neurons as well as “abnormally” located ones related to the occlusion, with the latter one located more distal to the TZ than the former ones (34-44). Histological procedures were then applied to both hemispheres to obtain 75 micrometers thick frontal serial sections of brain: (i) the animals were

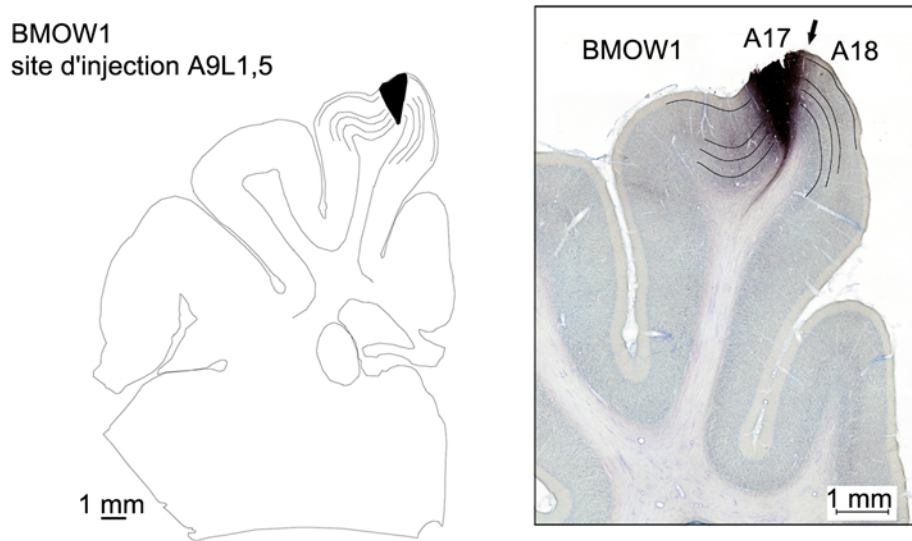


**Figure 1.** An example of a biocytin injection site in a MD cat (cat BMOW1). On the left, this injection site is represented as a camera lucida drawing. On the right, it is represented on a photomicrograph. The two views are shown in coronal sections of the left hemisphere. The region containing densely packed, labeled cell bodies and neuropil (the core of the injection) appears in solid black. The drawing represents the maximal extent of the injection site in 21 superposed adjacent sections (thickness, 75 micrometers). The core of the injection extended along the antero-posterior axis over 1575 micrometers; it aimed at labeling callosal axons originating the transition zone between A17 and A18 (TZ). In the photomicrograph, continuous lines denote the limits of the different cortical layers (I to VI). The arrowhead is centered on the TZ. Note that the part of the injection site extending below layer VI consists exclusively of densely packed axons labeled from the overlying cortex.

deeply anesthetized and then perfused transcardially with 0.1 M PBS at pH 7.4, and then with a mixture of 4% paraformaldehyde in PBS and 0.3% glutaraldehyde); (ii) brains were cryoprotected in a 30% sucrose solution, frozen sectioned and incubated at room temperature for 12 hours in an avidin peroxidase complex (ABC kit, 1/200 dilution into PBS solution with 1% of Triton-X100). A second incubation was performed in diaminobenzidine solution to stain peroxidase and amplified with nickel sulphate. Alternate frontal sections were Nissl stained for cortical layers identification. A17, A18 and the TZ in the primary visual cortex of each cat were identified by differences in cortical thickness (23-25). With the NeuroLucida® tracing system (MicroBrightfield Inc.) and the highest magnification (1200x, with oil immersion) of the brain sections, the three-dimensional morphology of individual callosal axons was then reconstructed from the midline to their terminals in the *right hemisphere* i.e. ipsilaterally to the occluded eye. For detailed methods for the 3D reconstruction and the quantification of morphology of these axons using the Neuroexplorer program (concerning nodes, branches etc...), refer to Houzel and collaborators (1). Histological procedures such as fixation, cryogenation, defatting and mounting on slides generally induce a 35-40% isotropic shrinkage along the *x*, *y* and *w* axes. Compression of the tissue also occurs perpendicular to the cut surface of sections, reducing section thickness by ~1/3 of its value at the time of sectioning. Both were compensated appropriately in numerical data analyses (incrementing by 35% and 33% for shrinkage and compression respectively), thus improving the precision of

the quantitative data of the reconstructed in 3D axons (cf. ref. 2 for details).

### 3.1.4. Axonal morphology

The morphology of each callosal axon that was reconstructed in 3D from the visual cortex of MD animals was characterized on the basis of criteria that we have previously described to characterize callosal axons in normally reared (NR) adult cats (1). This facilitated the comparisons between MD and NR groups. In summary (see Figure 2), the *trunk* is identified as that part of the axon proximal to the first branching point (*node*). The part of the axon located distal to the first node is called the *terminal arbor*. Axonal branches are then identified by their topological order. Thus, *first-order* (or *primary*) branches originate from the first node and that give rise to the *second-order* (or *secondary*) branches; the latter give rise to *third-order* (or *tertiary*) branches, etc. Branches which were particularly conspicuous by their length and/or thickness were designated as *main branches*. *Preterminal branches* carried (presumably synaptic) boutons. The latter could be *terminal boutons*, characterized by the presence of a connecting stalk or "*en passant*" boutons, i.e. swellings along the pre-terminal branch.

In the grey matter, axons may end with one or several *tufts*. A *tuft* is a part of an arbor characterized by densely ramified and tightly distributed high-order and pre-terminal branches originating from a common stem. In addition, they may have some modest *collaterals*. Tufts and/or collaterals of one axon may terminate in segregated volumes of cortex including one of several cortical layers.

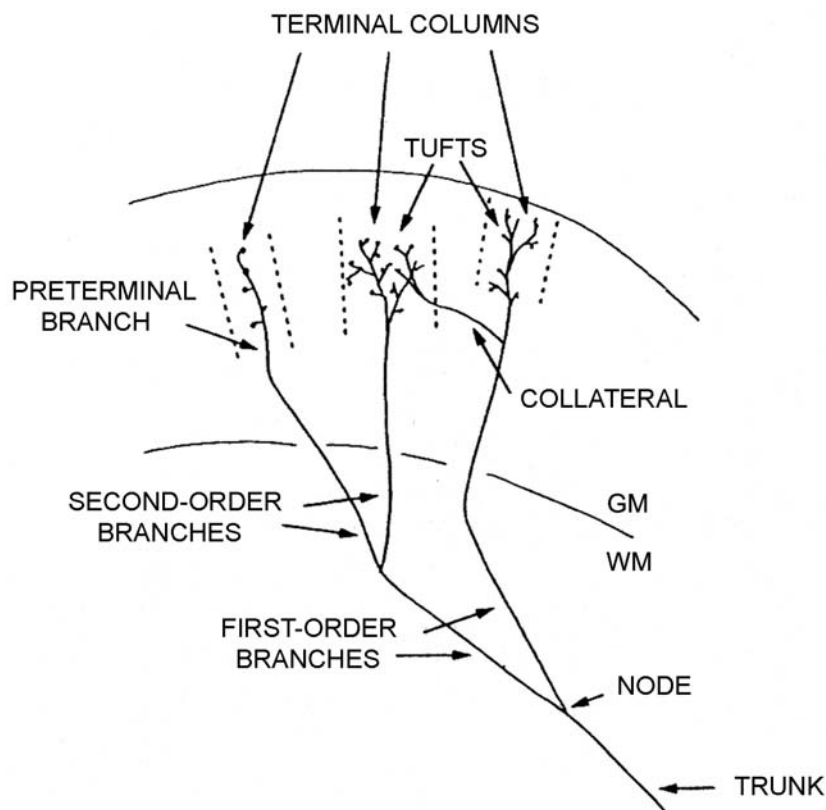


**Figure 2.** Schematic drawing of a terminal arbor ending in the cerebral cortex (VM = white matter, GM = grey matter) and illustrating the nomenclature employed. ‘Terminal columns’ refers to the volumes delineated by interrupted lines; the column at left is supplied by an isolated pre-terminal branch. For further details, see text (Reproduced with permission from ref 1).

Hereafter we call these volumes *terminal columns*. The characterization of a terminal column requires the identification of distinct *clusters* of *pre-terminal branches* and *boutons* in a view perpendicular to the cortical surface.

### 3.1.5. Architecture of individual terminal arbors

Axons may vary in the complexity and spatial organization of their terminal arbors. On the basis of data we have previously obtained in NR adults, at least four types of architectures may be differentiated (Figure 3):

-*A simple architecture*: the axon terminates with a single tuft within an approximately conical volume (not shown);

-*A parallel architecture*: the axon usually divides in the white matter, and first- or higher-order branches of comparable lengths supply different cortical columns or converge onto the same column. These branches usually run close to one another over several mm (Figure 3A).

-*A serial architecture*: This is characterized by a trunk (or else a first- or higher-order branch) with roughly radial collaterals to the cortex. Usually, the tangential running trunk also has a larger caliber than the collaterals (Figure 3B).

-*A mixed serial-and-parallel architecture*: A typical example is presented in Figure 3C.

## 3.2. NUMERICAL SIMULATION

After 3D reconstruction of single callosal axons from MD animals with NeuroLucida software, data were exported to *NEURON* for simulations of the orthodromic propagation of spikes along these axons.

### 3.2.1. Importing anatomical data to *NEURON*

Morphological data were obtained using NeuroLucida (*MicroBrightfield, Inc.*) based on the image-combining microscope concept (45-46). Each NeuroLucida file stores informations about several features (axonal segments, bifurcations (or nodes), synaptic boutons, contours of sections, landmarks, etc). It is organized as a serially ordered list of instructions describing all steps of the tracing procedure. Morphological data can be then exported through ASCII files. Here, the data conversion from NeuroLucida ASCII files to a *NEURON* “HOC” file was performed through the CVAPP freeware (available at: <http://neuron.duke.edu/cells/download.html>). When imported in *NEURON* as a “HOC” file, the data describes the topological and geometrical structures of the arbors which are represented as segments upon which simulations of the dynamics of the membrane potentials can be performed. During the conversion procedure, the data must be carefully checked and any possible conversion and/or interpretation errors must be corrected. Because this resembles the procedure for export from NeuroLucida to

**Cortical synchrony and abnormal visual experience**

**Table 1.** Quantitative analysis of the callosal terminal arbors in MD and NR animals

		<b>MD</b>	<b>NR</b>	<b>STAT</b>
<b>N axons</b>		9 to 10	15 to 17	-
<b>Architecture of callosal axons</b>	Axon branching* first very deep below the cortex	7/10	1/17	
	Simple	2	2	-
	Parallel	3	7	
	Serial	1	2	
	Mixed	4	4	
<b>Mean diameter +/- standard deviation (SD), with minimum and maximal values into brackets (in micrometers)</b>	Trunk*	1.7 +/- 0.5	1.2 +/- 0.3	P = 0.0166
		(0.87-2.68)	(0.65-2.02)	Z = 2.396
	1 <sup>st</sup> order branches	1.1 +/- 0.4	0.8 +/- 0.4	P = 0.0625
		- 35%	- 33 %	No Z value
	2 <sup>nd</sup> order branches	0.8 +/- 0.5	0.7 +/- 0.4	
		- 53 %	- 42 %	
	3 <sup>rd</sup> order branches	0.6 +/- 0.3	0.5 +/- 0.3	
		- 65 %	- 58 %	
	4 <sup>th</sup> order branches	0.5 +/- 0.3	0.5 +/- 0.3	
		- 71 %	- 58 %	
	5 <sup>th</sup> order branches	0.4 +/- 0.3	0.4 +/- 0.3	
		- 77 %	- 67%	
<b>Mean length of the branches +/- SD (in micrometers)</b>	1 <sup>st</sup> order branches	2895 +/- 2040	1599 +/- 1366	P = 0.1195
				Z = 1.5569
	2 <sup>nd</sup> order branches	752 +/- 819	433 +/- 494	P = 0.2458
				Z = 1.1606
	3 <sup>rd</sup> order branches	356 +/- 207	253 +/- 236	P = 0.2235
				Z = 1.2172
	4 <sup>th</sup> order branches*	484 +/- 308	132 +/- 76	P = 7.56.e <sup>-0.4</sup>
				Z = 3.3685
	5 <sup>th</sup> order branches*	233 +/- 193	79 +/- 39	P = 0.0156
				Z = 2.4189
<b>Mean number of nodes +/- SD</b>		168 +/- 166	124 +/- 88	P = 0.9160
min and max values		4-535	18-299	Z = 0.1054
<b>Mean number of terminals +/- SD</b>		171 +/- 166	125 +/- 88	P = 0.8952
min and max values		5-536	19-300	Z = 0.1318
<b>Mean number of terminal boutons +/- SD</b>		604 +/- 546	307 +/- 247	P = 0.1965
min and max values		8-1748	33-864	Z = 1.2915

Parameters compared between experimental groups include the number of callosal axons as a function of their architecture (simple, parallel, serial, mixed), the number of axons with a first node very deep below cortex, the mean diameter of their trunk (with minimum and maximum values), the mean diameter and the mean length of the first five order branches, the mean number of nodes, the mean number of terminals and of terminal boutons (again with their respective minimum and maximal values). The percentages below the mean diameters of the first five order branches correspond to the mean decreases of their diameters with respect to that of the trunks (whose mean diameters were taken as a reference, i.e. 100%). For statistical analysis (STAT column), we generally used a Wilcoxon rank sum test which performs a two-sided rank sum test for two independent unequal-sized samples. But for comparing the decrease in percentage of the mean diameter of the 1<sup>st</sup> to 5<sup>th</sup> order branches, we used a Wilcoxon matched-pairs signed-ranks test (W2) which compares pairs of values (cf. 75-76). Asterisks indicate significant differences between both groups. See text for details.

## Cortical synchrony and abnormal visual experience

**Table 2.** Comparison of properties of individual callosal axons and timing of spike arrivals within their respective terminals in normally reared (NR) animals and early monocularly deprived (MD) animals

		TRUNK				TIMING				
		Length	Mean diameter	Spike velocity	Trunk timing	Number of terminals	Mean terminal diameter	Mean arrival time at terminals	Time dispersion (ms)	
	Axon name	Micro-meters	Micro-meters	m.s <sup>-1</sup>	ms		Micro-meters	ms	2*sigma	Range max-min
NR	EN16H	3803	1,12	8,0	0,47	90	0,2	<b>0,90</b>	0,1	<b>0,2</b>
	EN22B	10121	0,66	4,7	2,15	183	0,22	<b>3,51</b>	0,6	<b>1,5</b>
MD	BMOW1.1	9558	1,68	12,0	0,79	27	0,35	<b>2,10</b>	0,7	<b>1,5</b>
	BMOW1.2	9653	1,68	12,0	0,80	252	0,3	<b>1,75</b>	0,8	<b>1,8</b>
	BMOW2.1	9839	2,16	15,4	0,64	60	0,2	<b>1,70</b>	0,2	<b>0,7</b>
	BMOW2.3	10532	2,04	14,6	0,72	83	0,4	<b>1,37</b>	0,4	<b>1,2</b>
	BMO17A1	14359	0,87	6,2	2,31	49	0,15	<b>3,00</b>	0,6	<b>0,9</b>
	BMO17A2	13759	1,39	9,9	1,39	243	0,15	<b>2,40</b>	0,7	<b>2,7</b>
	BMO17A3	12105	1,53	10,9	1,11	106	0,16	<b>2,60</b>	0,8	<b>2,1</b>

The trunk properties (length and diameter) of each axon are reported in the 3<sup>rd</sup> and the 4<sup>th</sup> columns. The theoretical estimation of spike velocity and traveling time in these different trunks are then reported in the 5<sup>th</sup> and the 6<sup>th</sup> columns respectively. The 7<sup>th</sup> to 8<sup>th</sup> column concern terminal morphology, reporting the number of terminals for each axon and their mean diameters. The last three columns show the timing of spikes arrivals at the end of each terminal: their means, twice their standard deviation and their range (max-min). The standard deviation is doubled to help compare their values with the range value and to estimate the dispersion.

*MAXSIM* software, the paper from Tettoni and collaborators may be used as a reference for further details (47).

### 3.2.2. Model assumptions and procedure

As mentioned above, in order to simulate the spike propagation in callosal axons of NR cat visual cortex, Innocenti and colleagues used a model where the propagation had a constant velocity in each segment as determined by its constant diameter (*MAXSIM software*, c.f. ref. 2). Here, to perform our simulations in callosal axons of MD cat visual cortex, we instead chose *NEURON software* because it is based on a compartmental model (see ref. 48 for a comparative review). This was expected to provide more flexibility for controlling the biophysical parameters relevant for spike propagation and timing such as membrane capacitance, axial resistance and distribution of voltage-dependent channels. However, this choice was accompanied by certain difficulties due to the likely myelination of at least the largest branches of the callosal axons under study, and it was necessary to find solutions to simulate the effects of this on propagation speed. Electron microscopy studies have revealed that branches of callosal axons with diameters greater than 0.25-0.3 micrometers are myelinated in adult cats (49-50; see also below). Note that the diameters of the axon trunks reported here are all superior to this value (see Table 2). It has also been shown that early monocular deprivation has little effect upon the development of myelinated fibers (51) and upon the expression patterns of myelination genes (52). Furthermore we have reported that the distribution of glial cells (here astrocytes), their morphology and the timing of their development are similar both in NR and MD cats, from two postnatal weeks to adulthood (53-54). Similar results have been obtained in monkeys for astrocytes, microglia and also for oligodendrocytes which constitute the myelin sheath of

axons (55). Thus, while myelination was not confirmed in the MD group here, these studies indicate this should be normal.

The myelin sheath increases the spike propagation velocity  $V_s$  by dramatically decreasing the membrane capacitance, and thus increasing the passive diffusion constant  $D$  of the fiber. In addition, myelination may change the type of propagation from a continuous locally regenerative conduction to a discrete saltatory one. In vertebrates, the spike regeneration occurs at hot spot nodes with high concentrations of  $Na^+$  channels and separated by a certain inter-nodal distance  $\lambda$  (56). In the mammalian central nervous system, the inter-nodal distances vary from 0.1 mm to 3 mm and the density of  $Na^+$  channels ranges from 1,000 to 10 000 units/micrometers<sup>2</sup> at nodes (57-58). In addition, the inter-nodal distance is not constant in cortical axons, particularly near bifurcations (59).

The effect of branching nodes on spike propagation in myelinated axons rises to an additional problem. This was first studied with computational models by Zhou and Chiu (60). A compartmental model of the myelin sheet should contain several compartments for each inter-nodal segment (one compartment for each layer), plus a compartment at each node (61-62). It is possible to construct compartmental models of realistic myelinated axons by using additional modules implemented in *NEURON* (63). However in the current literature, only single segments or single branching nodes were studied and the implementation of this method on complete arbors has not yet been reported perhaps because of the complexity of the problem as well as because of a lack of detailed in knowledge about myelin structure, internodes and so on.

In the present work, spike propagation was simulated on the basis of a homogeneous distribution of

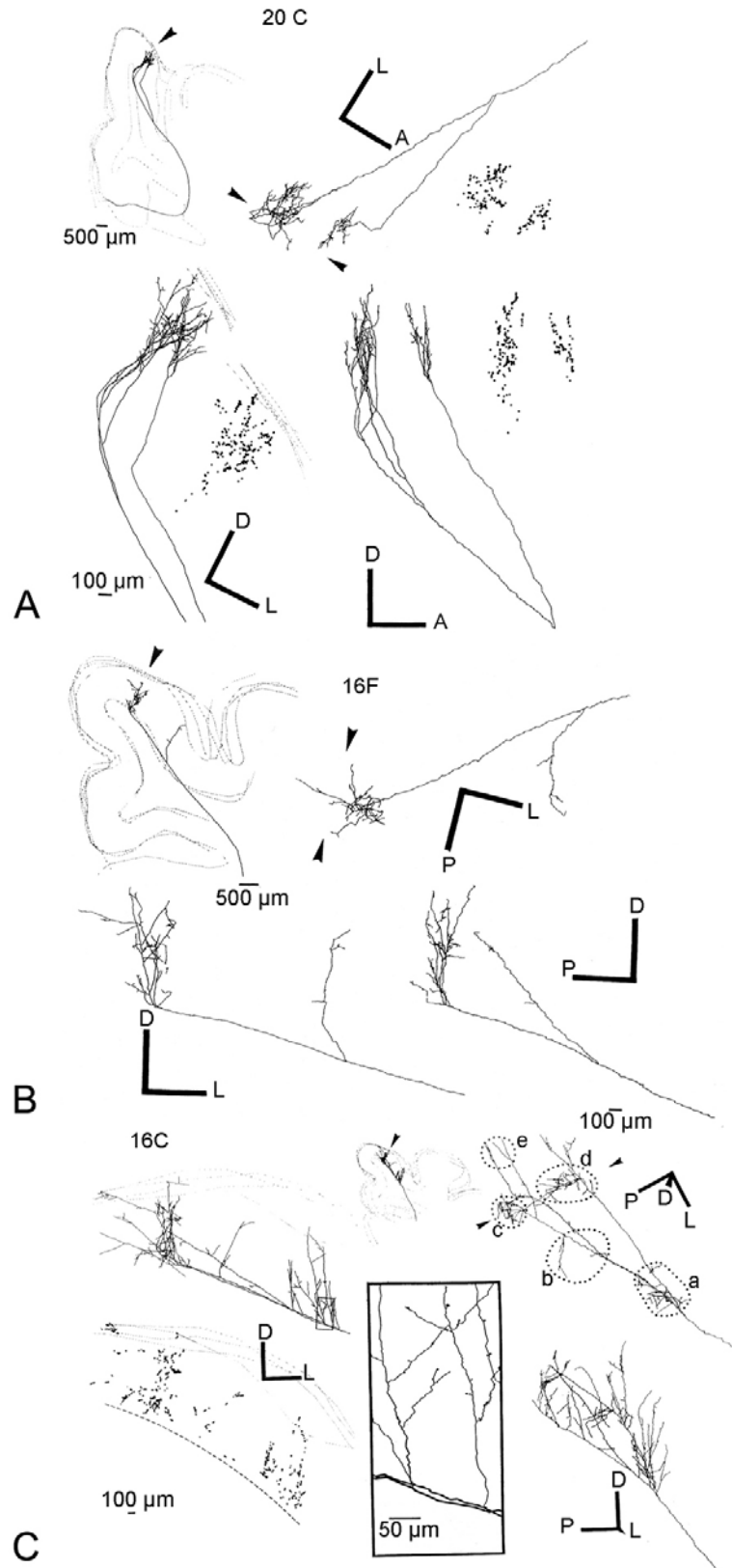


**Figure 3.** Different types of architectures of individual terminal arbors. A. Parallel architecture. B. Serial architecture. C. Mixed serial-and-parallel architecture (Reproduced with permission from ref 1).

## Cortical synchrony and abnormal visual experience

electrophysiological parameters as in the Hodgkin and Huxley model (HH). However, parameters in this model were adapted to simulate single spike propagation depending on whether the individual branches of each axon were myelinated or not. On the basis of data obtained by electron microscopy, we considered all our reconstructed axons to be myelinated at the level of their trunks since their diameters exceeded the 75<sup>th</sup> percentile (i.e. 0.41 micrometers) reported for non-myelinated fibers in adult cats (50). Wang and colleagues gave similar results for cat callosal axons (64). Therefore we assumed that the trunk of each axon was myelinated, and the myelination was considered to be effective for axon diameters greater than 0.28 micrometers (59-65-66). Indeed, although non-myelinated fibers in the CC of cat may range between 0.07 and 0.85 micrometers in diameter, smallest diameters are much more frequently observed in the range of 0.28 to 0.32 micrometers. In agreement with current models of spike propagation, the transition from myelinated to non-myelinated segments was modeled as a sudden jump in membrane capacitance and a continuous decrease in axial resistance, as detailed below (67-68).

### 3.2.2.1. The continuous model of Hodgkin and Huxley (HH)

The spatial and temporal evolution of the membrane potential in a continuous system depends on the standard cable equation:

$$1/R \cdot d^2V/dx^2 = C \cdot dV/dt + I(V,t)$$

where  $V(x,t)$  is the membrane potential at the spatial coordinate  $x$  at time  $t$ ,  $C \cdot dV/dt$  is the capacitive current and  $I(V,t)$  is the ionic current from inside to outside of the membrane, as conventionally reported.  $R$  is the axial resistance and  $C$  the membrane capacitance. The factor  $D=1/(RC)$  is the diffusion coefficient and the impulse velocity  $V_s$  is proportional to the square root of  $D$ .

In the HH model, the ionic current dynamic is governed by the following equation:

$$I(V,t) = \sum_i G_i \cdot f_i(V,t) \cdot (V - V_{(i)}) + G_L (V - V_{(L)})$$

where  $i$  is the index of each ionic channel (Na, K,...),  $G_i$  its ionic conductance,  $V_{(i)}$  the equilibrium potential of the channel and  $f_i = m_i^{k(i)} \cdot n_i^{l(i)} \dots$  a polynomial function of the probabilities  $m_i, n_i, \dots$  of state changes of the subunits of the channel. We added the leakage current  $G_L (V - V_{(L)})$  which was included in the generic formula with  $f_i$  constant. These quantities  $m_i, n_i, \dots$  satisfy differential equations involving  $V(t)$ . Conductances and equilibrium potentials are the main parameters of the channel that are set in the compartmental modeling software, where they control the local dynamics of the membrane potential.

In a non-myelinated system such as the HH model,  $C$  varies linearly with the axoplasm diameter (fiber inner diameter, i.e. without myelin)  $a$  and  $R$  varies as  $a^{-2}$ . As shown by Scott, the spike conduction velocity  $V_s$  is

proportional to the square root of the diffusion coefficient  $D=1/(RC)$  and thus proportional to the square root of  $a$  (68). This corroborates the increase in spike propagation velocity with  $a^{1/2}$  as first observed in the squid giant axon. For a myelinated system, parameters for this model were adapted (see below).

### 3.2.2.2. Effects of the myelin sheath on spike propagation

As found in many axons in vertebrates, the largest axons of the CC in cat are covered with an insulating sheath of myelin except at gaps called "nodes of Ranvier", where there is a high density of fast voltage dependant  $Na^+$  channels. The presence of such myelin sheath is known to drastically enhance the conduction velocity of spikes with two major changes in the axonal configuration: a) The multilayered insulation sheath of myelin greatly reduces the membrane capacitance; b) The presence of myelin localizes ionic channels mostly at the hotspots nodes of Ranvier.

As demonstrated by modeling the myelin sheath as thin concentric cylindrical capacitive shells and by integrating the inverse of individual capacitances of shells along the radii, the total capacitance becomes inversely proportional to  $\log(a_M/a)$ , where  $a_M$  is the outer diameter of the myelin sheath (67). However the ratio  $a_M/a$  has been experimentally found to be virtually constant. Thus, in the presence of myelin, the capacitance  $C$  may be kept constant independently of the axoplasm diameter. The diffusion coefficient  $D$  also becomes proportional to  $a^2$  and the propagation velocity  $V_s$  proportional to  $a$ . This is consistent with the fact that the spike propagation velocity in myelinated axons is proportional to  $a$ .

### 3.2.2.3. Transition from saltatory to continuous spike propagation

Several attempts have been made to build theories and models of the physiological properties of myelinated axons (see 68-69-70). They may be summarized as follows.

The basic model from Scott supposes the inter-nodal distance ( $\lambda$ ) to be constant (68). The inter-nodal resistance is supposed to be proportional to  $\lambda$  and is denoted by  $R$ , while  $C$  is the inter-nodal capacity of the membrane with myelin. Let us denote as  $n$  the index of nodes varying between 1 and  $N$ , the total number of nodes, and  $V_n(t)$  is the value of the membrane potential on node  $n$  at time  $t$ . The system of equations describing the voltage pulse propagation in a segment of myelinated fiber is a discrete reaction diffusion system described by a set of differential equations, coupling potentials and concentrations of various ions. The relation describing the membrane potentials between consecutive nodes is given by (c.f. ref. 68):

$$(1/R)(V_{n+1} - 2V_n + V_{n-1}) = C \cdot d(V_n)/dt + I_n(V_n, t)$$

where the term  $C \cdot d(V_n)/dt$  is the capacitive current and  $I_n$  the ionic current. This equation is coupled by the term  $I_n$  governing the states of the different channels.

## Cortical synchrony and abnormal visual experience

More elaborated models also introduce spike propagation in the myelinated segments (see 71). Nevertheless no complete model is yet able to reproduce quantitative data and only two asymptotic limits are well described:

- The “continuous limit” is defined when  $(V_{n+1} - V_n)/V_n$  is very small (i.e. much smaller than 1)
- The “saltatory limit” is defined when  $(V_{n+1} - V_n)/V_n$  is very large (i.e. much larger than 1)

Small values of  $\lambda$  lead to dynamics similar to those described by the *continuous limit* where the usual HH partial differential equations system closely approximates the discrete system. Large values of  $\lambda$  lead to systems showing propagation failure. In between, when the inter-nodal distance increases, a critical distance exists where saltatory propagation occurs. But neither the saltatory limit nor the continuous approximation gives satisfactory estimates of the impulse velocity in natural situation. Computational studies predict a range of values for  $\lambda$  giving a velocity close to the maximal value with almost no failure. Furthermore, experimental data report this optimal range of  $\lambda$  in many species including cats (for details and references, see ref. 68). The most important result for theoretical work as well as for numerical experiments was Moore and collaborators discovery that near the critical value, “the conduction velocity is insensitive to the inter-nodal length but much more sensitive to the myelin capacitance and axoplasm conductance” (71). This result is enlightened by the numerical calculations of Binczak and collaborators showing there is a maximal impulse velocity at a critical value and the velocity decreases slowly when  $\lambda$  decreases (72).

Thus, here, for the simulation of spike propagation into the large myelinated part of callosal axons, we hypothesized that it is possible to adapt the value of an impulse velocity by appropriately choosing the constants C and R with small values of  $\lambda$ , which allows us to use a continuous model under the following conditions: a) to obtain a spike propagation velocity proportional to the axoplasm diameter (instead of its square root), the experimental values of axoplasm diameters  $a_{\text{real}}$  are replaced by effective diameters  $a_{\text{eff}}$  proportional to their values squared, b) to maintain the correct physiological value for the axial resistance R while allowing to adjust the membrane capacitance C, c) to ensure that the effective diameter must vary continuously at the transitions between myelinated segments and non-myelinated terminal branches. Note that these conditions forces to adopt non-plausible values for C.

To achieve these conditions, we introduced a normalization factor ( $a_{\text{trans}} = 0.28$  micrometers) that corresponds to a threshold for axoplasm diameter where myelination is likely to cease (2). The transformation from the actual measured diameter of axoplasm ( $a_{\text{real}}$ ) and the effective diameter ( $a_{\text{eff}}$ ) for use in the continuous HH model simulation was as follows:

$$a_{\text{eff}} = a_{\text{real}}^2 / a_{\text{trans}}$$

### 3.2.2.4. Implementation of the model on the diverse real morphologies of callosal axons

An original advance here is propagation of spikes in both non-myelinated and myelinated parts of the same axon. Another innovation is analysis of the temporal dispersion in spike propagation through morphologically abnormal callosal axons. In computer simulations of the HH model based on the diameters provided by 3D reconstructions with NEURON, we assumed a homogenous distribution of channels which fixed the values of specific conductances, the reversal potentials, the axial resistance and the membrane capacitance. We performed simulations in a continuous mode with impulse velocity corresponding to the saltatory mode of spike propagation for segments with axonal diameters larger than  $a_{\text{trans}}$  (0.28 micrometers), and in the ordinary continuous mode of propagation for smaller diameter. The normal physiological parameters have been retained for terminal branches in order to reproduce the continuous spike propagation on these tiny elements whereas squared diameters and an adapted capacitance were set for the main branches in order to simulate fast saltatory propagation on the myelinated segments.

Following Spruston *et al.* and Johnston and Wu, the following values for specific conductances were provided to the HH model:  $G_{\text{Na}} = 0,250 \text{ S.cm}^{-2}$ ;  $G_{\text{K}} = 0,036 \text{ S.cm}^{-2}$ ;  $G_{\text{L}} = 166.10e-6 \text{ S.cm}^{-2}$  while the reversal potentials were  $V_{\text{Na}} = 71,5 \text{ mV}$ ;  $V_{\text{K}} = -89,1 \text{ mV}$ ;  $V_{\text{L}} = -60,0 \text{ mV}$  (73-74). The values for axial resistance and membrane capacitance were adjusted in order to recover the empirical relation between the spike velocity ( $V_s$ ) and the axon diameter on the myelinated parts. For mammalian myelinated fibers Waxman and Bennett have reported the following relation:  $V_s \text{ (m.s}^{-1}\text{)} = 7.14 \text{ areal (micrometers)}$ , where areal is the axoplasm diameter under experimental observation (65). The axial resistance was fixed at its actual value (123 ohm-cm) in order to preserve the natural continuity of the inner media of the axoplasm at the myelinated/non-myelinated transition. We then explored numerically the effect of varying membrane capacitance in linear segments on the ratio between the spike velocity and the axon diameter. We found that a constant value of  $0.150 \text{ microF.cm}^{-2}$ , which is smaller than the experimental value by about one order ( $1 \text{ microF.cm}^{-2}$ , c.f. 73-74, leads to the expected relation  $V_s = 7.14 a_{\text{real}}$ .

Finally, the simulation of current injection into a virtual soma connected to the initial segment increased the local membrane potential value to reach the spiking threshold and initiated the spike propagation (See Figure 4). The spike arrival times on each termination of the axon were computed from the onset of spike initiation at the first segment of the trunk. At termination, spike events were binary transformed by threshold analysis (-40 mV) and counted into bins with widths of 0.01 ms for histogram construction.

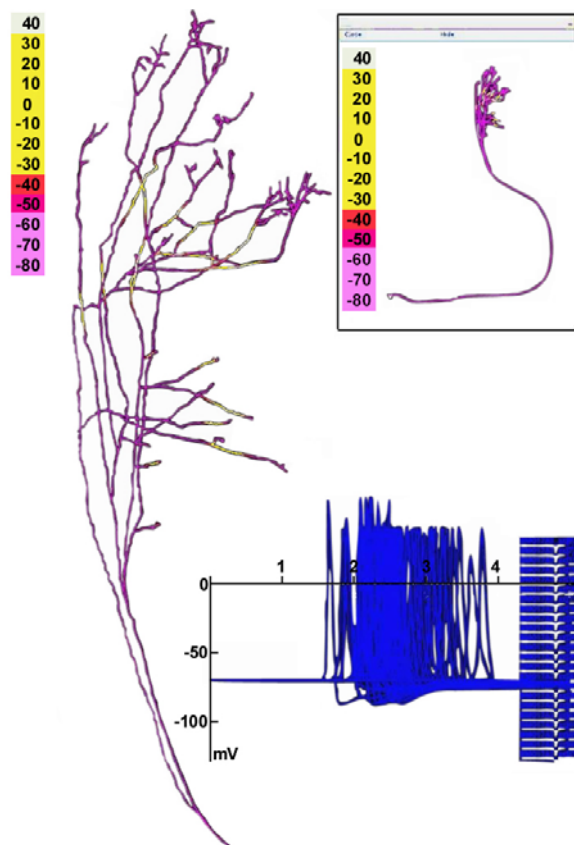


**Figure 4.** Screen capture of *NEURON* simulation. *On the left*, the figure illustrates the evolution of the membrane potential (in mV) along axon BMO17A3. *Insert:* complete morphology of this axon (see also Figure 5 for further details). *Below right*, simulated membrane potential (in mV) as a function of time (ms), with  $t_0$  corresponding to the initiation of a spike at the root of the axon: the various traces represent the spikes with the timing of their respective arrivals at the end of each branch of the arbor.

## 4. RESULTS

Here first some aspects of the anatomy of the callosal axons which have been reconstructed in 3D from early monocularly deprived (MD) animals will be described. Then, the data resulting from the simulation of the orthodromic spike propagation in these axons will be presented. Data from these two approaches will be systematically compared to those obtained previously in NR animals (1-2).

### 4.1. Anatomical data

In the MD animals, ten callosal axons were labeled after injection of biocytin in the left hemisphere ipsilateral to the eye that remained open and then 3D-reconstructed in the right hemisphere ipsilateral to the occluded eye (Figure 5). Four axons were labeled after injection in the 17/18 transition zone (TZ): axons MD9A and MD9B (not shown) were labeled from a posterior injection ( $P_2L_2$ ) in cat MD9; axons BMOW1.1 and BMOW1.2 were labeled from an anterior injection ( $A_9L_{1,5}$ )

in cat BMOW1.2. Six additional callosal axons were labeled after injection of biocytin in A17: three of these axons were labeled after a posterior injection of biocytin ( $P_3L_1$ ) in cat BMO17 (BMO17.A1, BMO17.A2 and BMO17.A3 respectively); three others were labeled after a more anterior injection of biocytin ( $A_4L_1$ ) in cat BMOW2 (BMOW2.1, BMOW2.2. and BMOW2.3 respectively). For comparison, callosal axons that were reconstructed in 3D in NR animals are shown in Figure 6.

The tangential and radial distributions of the terminals (including the terminal boutons) of these MD callosal axons in cat visual cortex, depending on their origin in the contralateral hemisphere, will be described into detail and compared to NR data elsewhere (Milleret *et al.*, in preparation; Foubert *et al.*, in preparation). Here, while all ten axons were considered together, only the data of interest for understanding the timing of callosal transmission in visual cortex will be presented. This includes their trajectories toward and within the lateral gyrus, their respective global architectures, the diameters and the lengths of their main branches (including the trunk), their respective numbers of nodes, terminals and boutons. These data will be compared to those of NR animals (Figure 5 to 8; Table 1 and Table 2).

#### 4.1.1. Location of the labeled axons in the corpus callosum

Labeled axons were routed unbundled through the dorsal half of the splenium of the CC. After entering the medial wall of the hemisphere they coursed below the bottom of the splenial cortex and then laterally and dorsally in the optic radiations. The average length of the trunk of the 3D-reconstructed callosal axons measured from a given starting point in the corpus callosum (generally the midline) to the bottom of layer I ranged between 19 and 88.6 mm. Both the distribution and the lengths of the labeled callosal axons were similar to those in NR adults.

#### 4.1.2. Global organization of the MD callosal axons

**4.1.2.1. Location of the first node of the MD callosal axons.** Callosal axons in MD animals could branch first at one of the three following positions: very deep in the white matter below cortex (while just exiting the CC), just below cortex or within the visual cortex itself (Figure 5). But these did not occur at equal incidences. Those branching first *very deep* below cortex were clearly the most numerous (7/10; cf. Table1). Most often, they branched as far as the level of the fundus of the splenial sulcus (s.s.) or that of the cingular sulcus (c.s.), depending of the antero-posterior position (see for examples axons MD9A, BMOW1.2 and BMOW2.3).

In the NR adults, all three types of callosal axons (described above) have also been found (Figure 6; cf. also Table 1). But only one branched first rather deep in the white matter (Axon 16E, Figure 6). For the 16 remaining axons, the first node was located invariably nearer the visual cortex, between the fundus of the lateral sulcus and the convexity of the lateral and post-lateral gyri, often beneath A18, or within the cortex itself. This significant difference is a first element indicating that the morphology

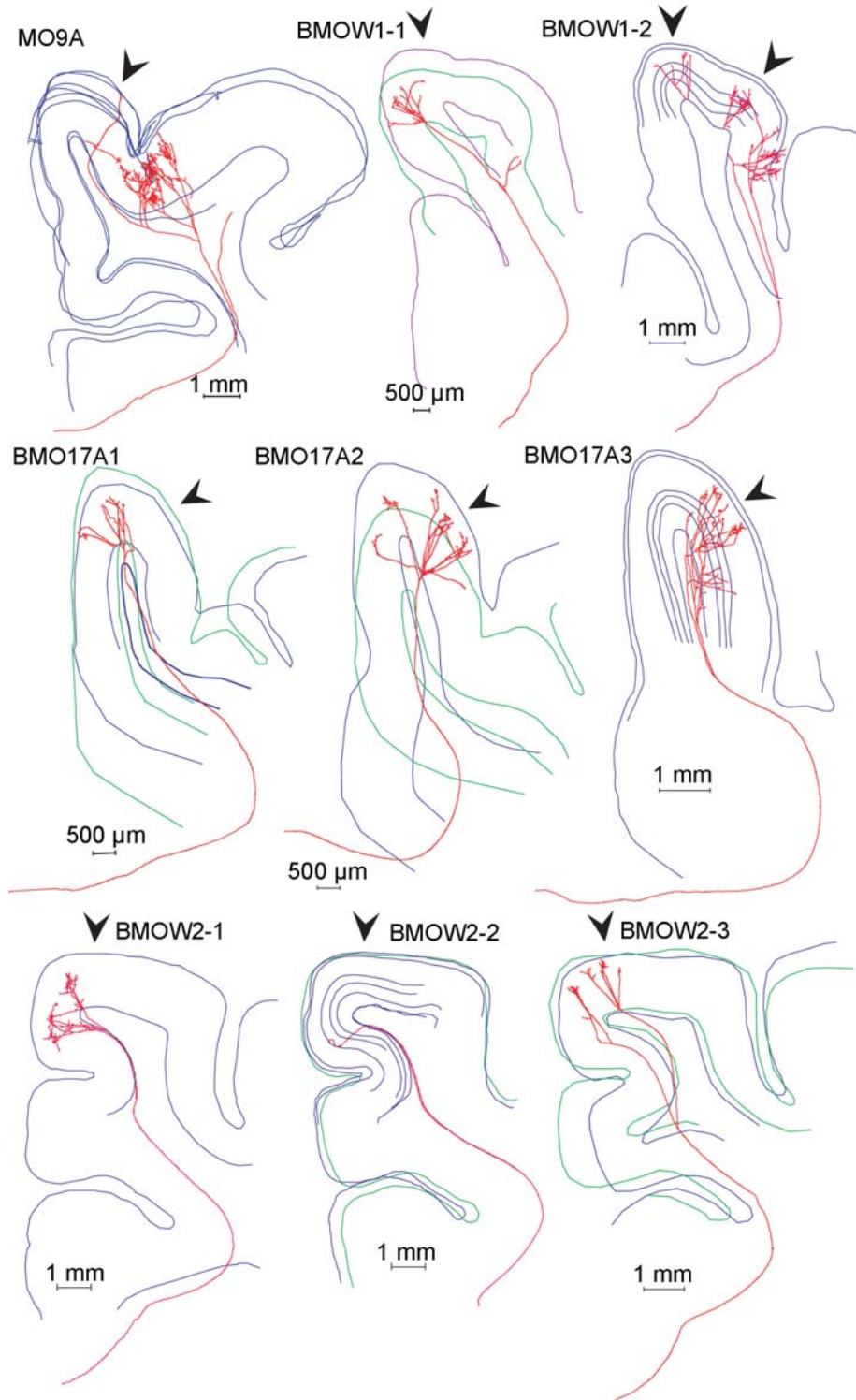


**Figure 5.** Computed-aided 3-D reconstructions of individual labeled callosal axons in early monocularly deprived (MD) animals. Code numbers refer to each cat. Each panel shows an axon within the outlines of a few serial sections (coronal sections of the right hemisphere seen from the posterior) used for the reconstruction; pial surface and bottom of grey matter are indicated by interrupted lines. Dorsal is upwards, medial to the left. Calibrations bars are 500 micrometers. Arrowheads are centered on the transition zone between A17 and A18; for one axon, the 18/19 transition zone is also indicated.

Cortical synchrony and abnormal visual experience

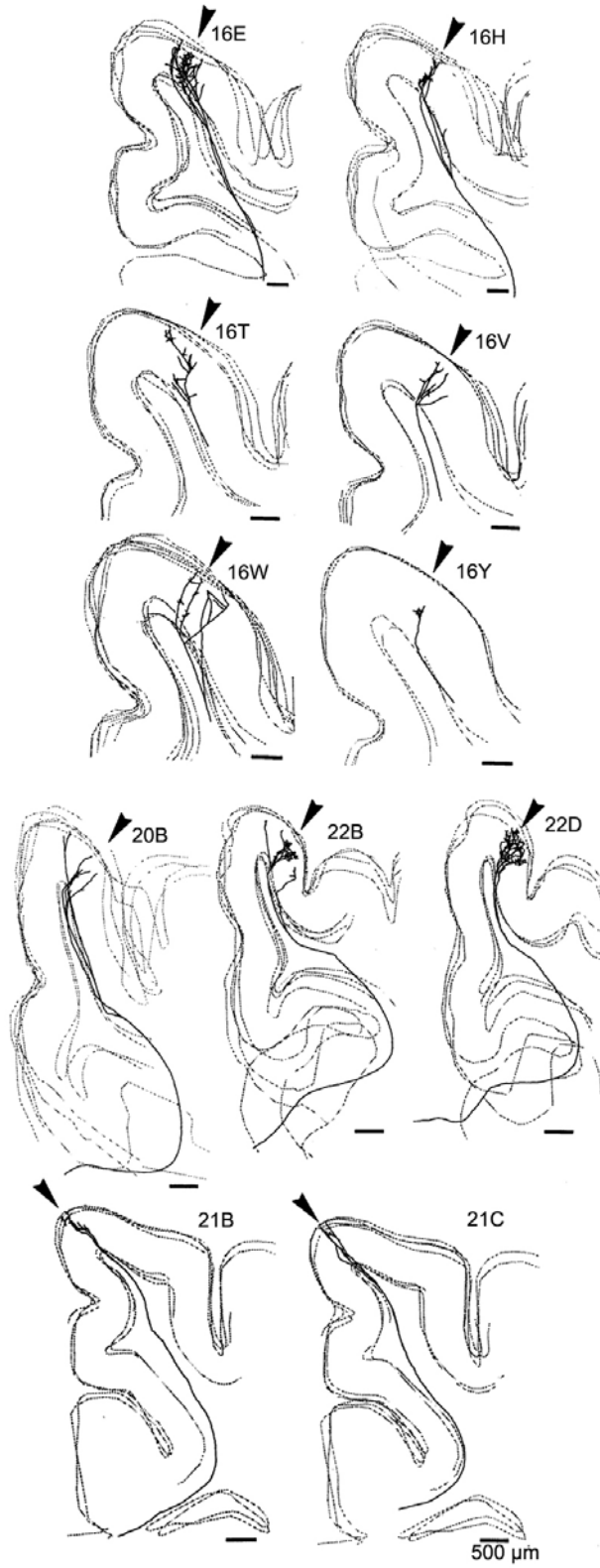


**Figure 6.** Computed-aided 3-D reconstructions of individual labeled callosal axons in normally-reared (NR) animals. Same legend as in Figure 5 (Reproduced with permission from ref 1).

## Cortical synchrony and abnormal visual experience

of the callosal axons is rather different in MD and NR animals.

### 4.1.2.2. Architecture of callosal terminal axons

On the basis of our classification (cf. “Materials and Methods”), out of the 10 MD callosal axons: 2 axons displayed a *simple* architecture (20%), 3 displayed a *parallel* one (30%), 1 displayed a *serial* organization (10%) and the 4 others displayed a *mixed* architecture (40%). In the NR adults, out of the 15 callosal axons that have been 3D-reconstructed and for which architecture was defined: 2 had a *simple* architecture (13%), 7 displayed a *parallel* one (47%), 2 were *serial* (13%) and the 4 remaining ones displayed a *mixed* organization (27%). Although the number of callosal axons is rather low, it can be at least concluded that the 4 architectures of the callosal terminal axons that have been found in NR animals are still present in MD animals. By contrast, it was not possible to determine statistically whether their respective proportions were modified significantly by the early monocular occlusion.

### 4.1.3. Quantitative analysis of the MD callosal axons

#### 4.1.3.1. Diameters of the trunks of the callosal axons

The mean diameter of the trunk of the reconstructed axons in MD animals was 1.7 +/- 0.5 micrometers, and ranged between 0.87 and 2.68 micrometers (Table 1; see also Table 2 for details about individual axons). The diameters did not seem to vary greatly depending on whether they originated in the TZ (cats MD9 and BMOW1; mean = 1.84 micrometers) or A17 (cats BMO17 and BMOW2; mean=1.61 micrometers). In order to determine whether the values for reconstructed axons were representative of the full range of axons originating near the TZ or from A17, 139 labeled axons were measured for callosal axons that ran towards the lateral gyrus, when exiting the CC. They were distributed as follows by animal: MD9, n = 34; BMOW1, n= 42; BMO17, n=23; BMOW2, n=40. Globally, the axons ranged between 0.27 micrometers and 3.17 micrometers in diameter, with a majority between 0.41 and 1.68 micrometers in diameter (Figures 7A and 7B). Since those we have reconstructed in 3D ranged between 0.87 and 2.68 micrometers in diameter, this indicates that they were among the largest axons within the total population (see Figure 7). Note that, in general, the diameter remained constant right up to the first node. However, it did vary in a few cases. To limit the effects of such variations, the mean diameter was used here.

All these characteristics were very similar to those reported previously in NR animals (1), except that largest axons were favored in MD animals for 3D-reconstruction while they were not (at least apparently) in the NR ones (Figure 7C; see also Table 1).

#### 4.1.3.2. Mean numbers and mean diameters of the 1<sup>st</sup> to the 5<sup>th</sup> order branches of the callosal axons

In MD cats, all callosal axons that were reconstructed in 3D displayed only two 1<sup>st</sup> order branches. But the mean number of branches increased with order as

revealed by analyzing (for example) the first five order branches of these axons: 2<sup>nd</sup> order branches, m= 3.4 (n = 2 to 5); 3<sup>rd</sup> order branches, m = 6.6 (n = 2 to 12); 4<sup>th</sup> order branches, m = 11.3 (n = 4 to 24); 5<sup>th</sup> order branches, m = 17.6 (n = 0 to 32). By contrast, their mean diameter decreased progressively with respect to that of the trunk (1.7 +/- 0.5 micrometers) as the order increased (cf. Table 1): 1<sup>st</sup> order branches, m = 1.1 +/- 0.4 micrometers; 2<sup>nd</sup> order branches, m= 0.8 +/- 0.5 micrometers; 3<sup>rd</sup> order branches, m = 0.6 +/- 0.3 micrometers; 4<sup>th</sup> order branches, m = 0.5 +/- 0.3 micrometers; 5<sup>th</sup> order branches, m = 0.4 +/- 0.3 micrometers. By taking the diameter of the trunk as a reference value, these decreases were 35%, 53%, 65%, 71% and 77% from the 1<sup>st</sup> to the 5<sup>th</sup> order respectively.

In the NR adults, data were very similar to that in MD cats, as assessed statistically using a Wilcoxon matched-pairs signed-ranks test (see 75-76 for details). Every callosal axon also systematically displayed only two 1<sup>st</sup> order branches. The mean number of higher order branches increased progressively in the same range as in MD animals: 2<sup>nd</sup> order branches, m= 3.75 (n = 2 to 4); 3<sup>rd</sup> order branches, m = 6.8 (n = 4 to 8); 4<sup>th</sup> order branches, m = 10.6 (n = 4 to 16); 5<sup>th</sup> order branches, m = 14.25 (n = 4 to 22). Mean diameters also decreased progressively relative to the trunk (1.2 +/- 0.3 micrometers) while the order increased and this occurred in the same range as the one that was observed after MD: 1<sup>st</sup> order branches, m = 0.8 +/- 0.4 micrometers; 2<sup>nd</sup> order branches, m= 0.7 +/- 0.4 micrometers; 3<sup>rd</sup> order branches, m = 0.5 +/- 0.3 micrometers; 4<sup>th</sup> order branches, m = 0.5 +/- 0.3 micrometers; 5<sup>th</sup> order branches, m = 0.4 +/- 0.3 micrometers (cf. Table 1). Again taking the diameter of the trunk as a reference value, these decreases were 35%, 53%, 65%, 71% and 77% respectively. Globally, this indicates that MD modified neither the number of the 1<sup>st</sup> to 5<sup>th</sup> order branches nor their diameter compared to normal subjects.

#### 4.1.3.3. Mean lengths of the 1<sup>st</sup> to the 5<sup>th</sup> order branches of the callosal axons

For this measure, the greatest deviations were found between MD and NR groups. The mean length of the 1<sup>st</sup> to the 5<sup>th</sup> order branches in MD animals were respectively: 2895 +/- 2040, 752 +/- 819, 356 +/- 207, 484 +/- 308 and 233 +/- 193 micrometers. In the NR animals, they were respectively: 1599 +/- 1366, 433 +/- 494, 253 +/- 236, 132 +/- 76 and 79 +/- 39 micrometers. The Wilcoxon test (see Table 1 for details) revealed that the length of the 1<sup>st</sup> to the 3<sup>rd</sup> order branches were very similar both in MD and NR animals. By contrast, the 4<sup>th</sup> and the 5<sup>th</sup> order branches were significantly longer after early monocular occlusion (multiplied by a factor of at least 3 compared to normal). Altogether, this leads to the conclusion that the length of at least some callosal branches was increased significantly in MD animals.

#### 4.1.3.4. Mean number of nodes of the callosal axons

The mean number of nodes per axon in MD animals was 168 +/- 166, ranging from 4 to 535. In the NR animals, the mean number of nodes per axon was 124 +/- 88, with a minimum of 18 and a maximum of 299. Comparing the groups revealed no significant differences

Cortical synchrony and abnormal visual experience

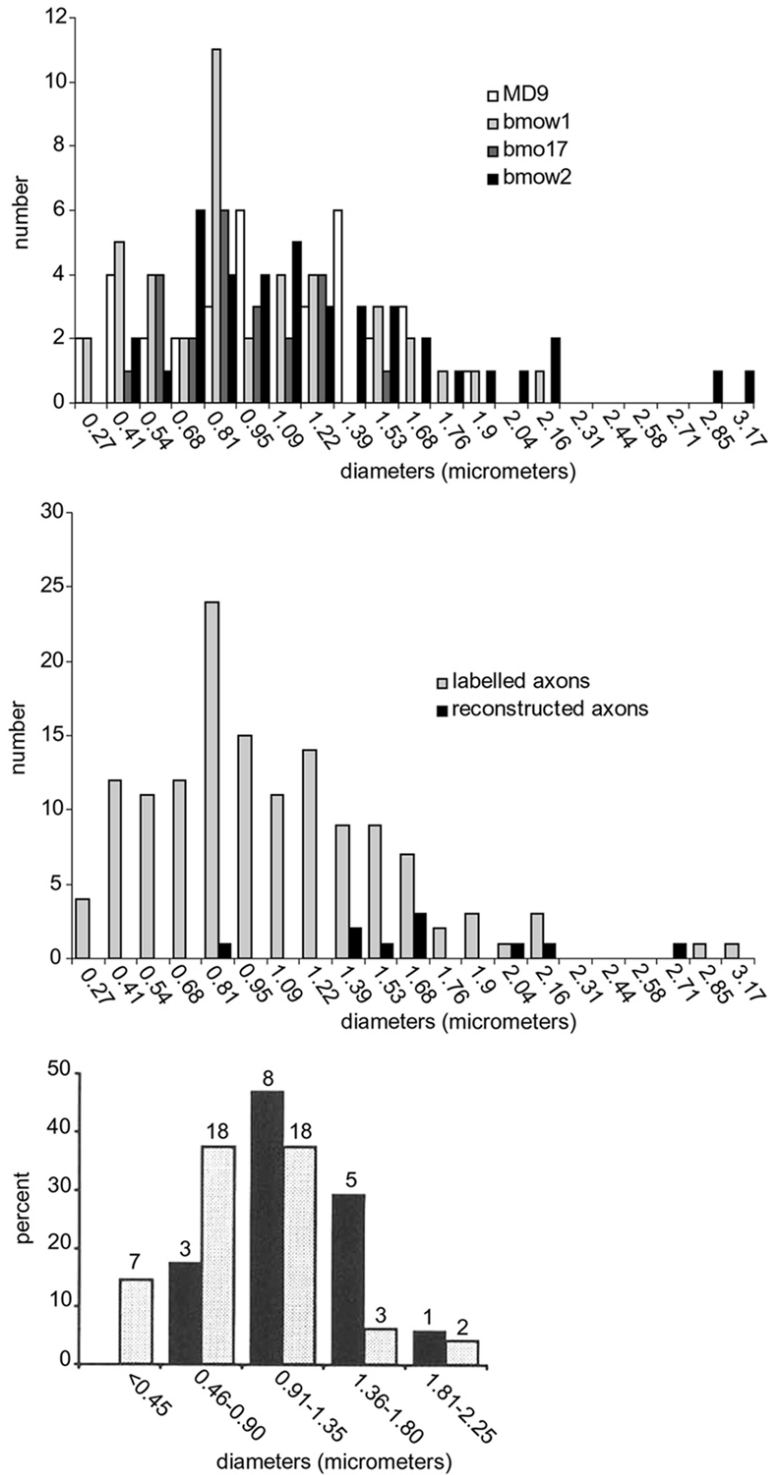


**Figure 7.** Summary histograms of the diameters that have been measured in the four MD cats (MD9, BMOW1, BMO17 and BMOW2). A. The 4 histograms (one for each cat). B. Combined histogram of data from all four MD cats, with the diameters of 139 axons that were measured. In black are indicated the 10 axons that were reconstructed in 3D here (MD9A, MD9B, BMOW1.1., BMOW1.2., BMO17.1, BMO17.2, BMO17.3, BMOW2.1., BMOW2.2., BMOW2.3.). C. Diameters of axons that were measured (in grey) and 3D-reconstructed (in black) in the NR adult cats (Reproduced with permission from ref 1).

(Wilcoxon test,  $P = 0.916$  and  $Z = 0.1054$ ; see Table 1). Note however these values had a tendency to be higher in MD animals (even if this was not significant with respect to the usual criterion of  $P = 0.95$ ).

#### 4.1.3.5. Mean number of terminals of the callosal axons

The observations about the numbers of nodes present within the callosal axons also held true for the callosal terminal branches. Globally, their mean number per axon was  $171 \pm 166$  in MD animals (range 5-536). In the NR animals, this mean number per axon was  $125 \pm 88$  (range 19-300). Again, although the difference between groups was not significant (Wilcoxon test,  $P = 0.8952$ ,  $Z = 0.1318$ ; see Table 1), this number had a tendency to be higher in MD animals.

All these callosal terminals ended as *tufts* and *columns*. These structures could originate from single or distinct pre-terminal branches originating in the white matter or the grey matter. To identify such terminal columns required the identification of distinct *clusters* of pre-terminal branches and boutons in a view perpendicular to the cortical surface (cf. Materials and Methods). In MD animals, when an evaluation “by view” was possible, the *number of terminal columns* ranged between 2 and 8 according to the axon. In NR animals, with the same approach, this number ranged between 1 and 7. Thus, the number of columns seemed to be in the same range in both experimental groups. However, the number of axons with numerous terminal columns was significantly higher in MD animals than in NR ones (intentionally not detailed here). Again this indicates that the MD callosal axons have more complex morphology than those in NR subjects.

#### 4.1.3.6. Mean number of boutons of callosal axons

Finally, we compared the mean number of boutons of the callosal axons in both experimental groups. In MD group, the mean number was  $604 \pm 546$  (min = 8; max = 1748). In the NR group, this mean was  $307 \pm 247$  (min = 33; max. = 864). Similar to the number of nodes and of terminals, there was not any significant difference between groups concerning the mean number of the boutons (Wilcoxon test,  $P = 0.1965$ ,  $Z = 1.2915$ ; see Table 1). But all quantitative data were again superior in MD animals.

Although this point will not be developed here (since it does not pertain to the issue of spike transmission delays), it is to be noted that the boutons of the callosal axons in MD animals were generally distributed at the end of the terminals (see axon BMO17-A3 in Figure 8 as an example), as in normal animals.

## 4.2. Simulation of the propagation of spikes in MD callosal axons

The simulations of spike propagation were performed using *NEURON* software in seven axons reconstructed in 3D from the MD experimental group: BMOW1.1, BMOW1.2, BMOW2.1, BMOW2.3, BMO17A1, BMO17A2 and BMO17A3. The three remaining cases were not used because the quantitative data obtained from NeuroLucida were incomplete or because

they were too simple both with respect of architecture and number of boutons (see for example axon BMOW2.2.). A typical spatio-temporal profile of activation of an MD callosal axon (BMO17A3) is presented in Figure 4. A single action potential was first initiated at the origin of the reconstructed trunk (see Materials and Methods). Then, after conduction along the axon, spikes invaded all the branches of the entire terminal arbor. The variations of membrane potentials (in mV) relative to the arrival times of the spikes (in ms) at the end of the terminal arbor could then be determined. Figure 9 and Table 2 illustrate the arrival times of such spikes for the seven MD callosal axons. Note that the absolute time values are not relevant here since only some were reconstructed in 3D from the midline. Finally, the evolution of the potential on each terminal was charted in histograms after fixation of a given threshold ( $-40$  mV; see below).

This procedure was also applied in two axons obtained from NR adult animals, EN16H and EN22B (cf. Figure 6 for their general morphology). The first NR axon (EN16H) shows a simple structure and a weak spatial dispersion where spike timing within terminal branches provided an estimation of the smallest possible dispersion. We used the value given by this axon to have an idea of the lowest bound of dispersion in the NR axons population. The second NR axon (EN22B) was chosen from those used by Innocenti and collaborators to simulate spike propagation in normal callosal axons by using *MAXSIM* software (2). Data obtained after simulations using our method and *MAXSIM* software were in very good agreement, confirming the reliability of our method. We reported activation on the first terminal of this axon at 2.93 ms whereas the original work reported a value of 2.88. This lends credibility to the validity of our method as compared with the original one. More generally, both methods provide similar dispersion ranges (0.2 to 2.7 ms).

It was surprising to observe that, for the abnormal structures i.e. the MD callosal axons, the vast majority of spike time distributions, as estimated with standard deviations, was constrained within a sub-millisecond interval (cf. Figure 9; Table 2). The differences between the maximum and minimum time dispersions in MD animals were very similar to those reported for subjects with normal callosal connections (2): in both cases, they ranged from 0.3 to 2.7 ms. Nevertheless, very asymmetric structures such as BMOW1.2 and BMO17A3 or the presence of a tiny non-myelinated collateral such as the one in BMO17-A2 axon (cf. Figure 5) could lead to spike arrivals within the two following ms.

## 5. DISCUSSION

This study demonstrates that conditions for both intra- and inter-hemispheric neural synchrony may be preserved in visual cortex of adult mammals despite abnormal postnatal visual experience. Indeed, due to an early monocular occlusion, the ten callosal axons from adult cat visual cortex that were reconstructed here in 3D displayed abnormalities in their architecture. Nevertheless, simulation of the orthodromic propagation of single spikes

BMO17A3

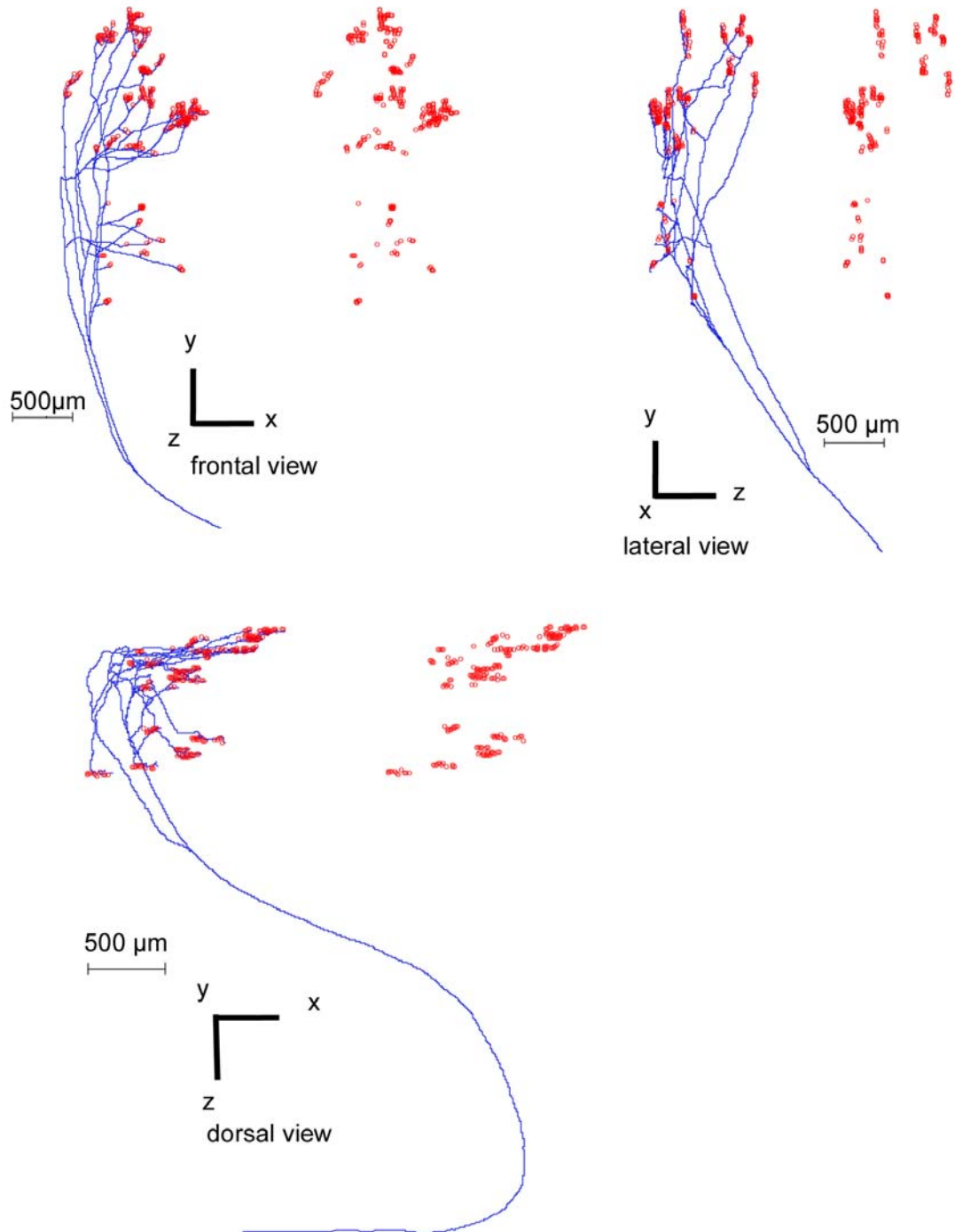


**Figure 8.** Illustration of a typical distribution of the terminal boutons of a single callosal neuron in the MD group. The reconstruction in 3D of a callosal terminal of the axon BMO17.A3 is represented here in three views: frontal, lateral and dorsal. In each view, the distribution of the terminals boutons is represented (in red) both within the callosal terminal itself and to the right of the arbor. Note that most of these boutons are located at the very end of the last branches of the axon.

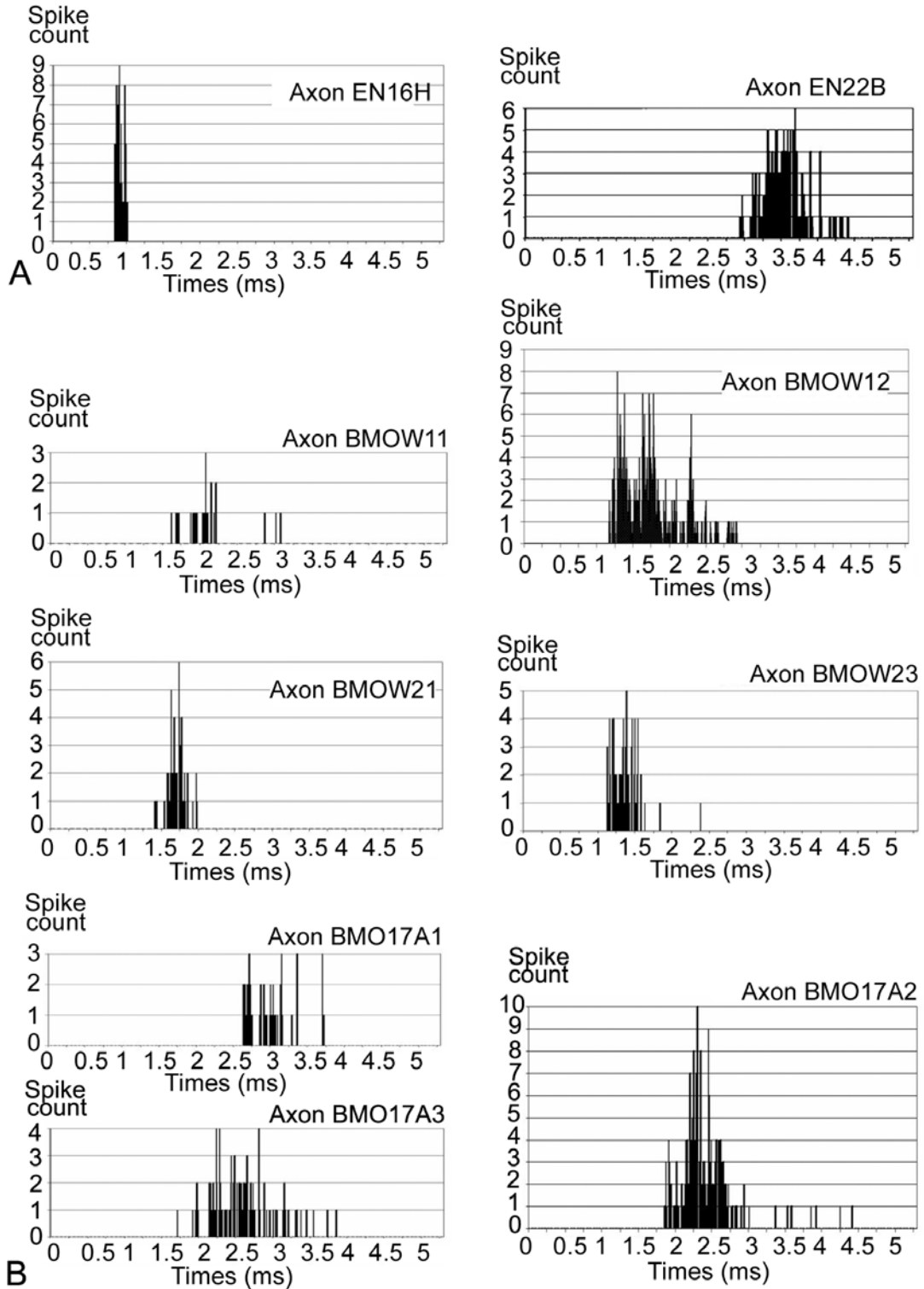


**Figure 9.** Histograms illustrating the dispersion of the arrival times of the spikes that are evoked within individual callosal terminals after simulation of one spike along the corresponding callosal axons. The two first panels on the top illustrate data that have been obtained for two callosal neurons in NR animals and serve as a reference (Axons EN16H and EN22B). The other panels below illustrate data that have been obtained for seven callosal axons in MD animals (Axons BMOW1.1., BMOW1.2, BMOW2.1, BMOW2.3, BMO17A1, BMO17A2, BMOW17A3).

along each of these axons (with *NEURON* software) revealed that almost all spikes arrived within a 3 ms interval at their terminals. This restricted time window corresponds to what is observed in the normal state. According to the temporal binding hypothesis, this implies that visual perception may occur normally in spite of anatomical abnormalities in visual cortex.

### 5.1. Effects of monocular occlusion on the morphology of callosal axons

Altering visual exposure of one eye during the critical period allows a juvenile-like widespread distribution of efferent callosal neurons throughout A17 and A18 to be maintained in the adult. This was observed repeatedly in various species (34-77-78-79-80-81). In contrast, little was known about the fate of callosal terminals in the other hemisphere under such circumstances, either globally or at the level of individual axons (36-82-83-84). Here, we analyzed the 3D morphology of single callosal arbors in 4-5 month old cats raised under monocular deprivation (MD) from the 6-7<sup>th</sup> postnatal day on, i.e. throughout the critical period. This demonstrated that MD also leads to substantial changes in the organization of the callosal terminal arbors within the hemisphere ipsilateral to the occluded eye. Since it is already known that such terminals establish functional synaptic contacts (35; Milleret *et al.*, in preparation) our data also suggest that some visual interhemispheric integration may occur in spite of such early deprivation.

We first showed that MD and NR axons did not differ significantly in their location in the CC, their trunk diameters (although only the largest ones were analyzed here), the diameter of their five first order branches and their principal architecture (with simple, parallel, serial and mixed axons in both cases). Note however that architectures could not be test for differences because of small data set. The number of terminal columns was in the same range in both groups (2-8 vs. 1-7 respectively) at least when determined by visual inspection. More surprisingly, the mean numbers of nodes, branches and boutons were not statistically different in the MD group as compared to the NR group. This was not expected because these parameters are classically considered as the main sources of changes in the architecture of axons in case of juvenile plasticity (e.g. 85). But each of these characteristics was numerically much higher in the MD group as compared to NR animals. This could have led to changes in the distribution of spike arrival times. However, our simulations based on the actual anatomical characteristics of each group demonstrate that this is not the case.

By contrast, the CC axons in MD animals differ very significantly from those observed in NR groups in at least two aspects. First, their first branching node was almost systematically located much deeper in the white matter than in NR animals. Second, some specific branches in the MD callosal arbors were significantly longer (multiplied at least by a factor 3) compared to normal. Concerning the first observation little is known about the mechanisms which determine the location of the first node of the callosal axons. We suspect however that some

clustered microglial cells located in the white matter below the visual cortex during the first post-natal month (i.e., when callosal axons develop) may be implicated in this. This is because these clusters are located precisely where the first callosal nodes are (cf. 53). We have also demonstrated that microglial cells within these clusters displayed an amoeboid morphology in the NR animals and a more ramified one in the MD ones. This suggests that they may participate to the elimination of callosal axons through a phagocytic activity in the NR group while they may favor sprouting of these axons by secreting nerve growth factors after MD. The second observation of an increase in length of some branches of the callosal terminals in MD subjects is likely the most interesting result of this anatomical study. To our knowledge, this is the first time that such a morphological change has been shown in callosal connections in visual cortex of adult mammal after vision has been modified early in life. Of interest, not all the branches increased in length: rather this occurred only from the 4<sup>th</sup> order branches. This indicates that such plasticity concerns some specific (the most distal) axonal branches only, and likely occurs within some specific cortical layers. While further work is in progress on this (Milleret *et al.*, in preparation; Foubert *et al.*, in preparation), interestingly, some literature already describes a differential susceptibility of supra- and infragranular cortical layers to sensory deprivation (e.g. 36-86-87-88). Note that only one other (recent) study has reported observations similar to these and they concern intracortical horizontal connections of MD animals which are also in relation with the non- deprived eye (89). Of interest, in contrast, diminution of some branches has been reported in visual cortex as a consequence of sensory deprivation (dark-rearing, 88; early MD, 89). This may be related to recent findings in visual system demonstrating a strong relation between axon branching related dynamics and correlated activity (39-41). By extension, this may also be related to the influence of synaptic maturation in visual cortex on axon branch dynamics (40-90).

### 5.2. Simulation of propagation of spikes along the callosal axons

The data allowing numerical characterization of the MD callosal axons were implemented in a simulation of spike propagation based on methods available from *NEURON software*. First, this software was chosen because it allows the use of physiological data. In particular, it allows simulation of different modes of spike propagation in the various segments. We intended to study the dispersion of times of spikes arrivals in the MD callosal terminals which include both myelinated and non myelinated branches, with the latter ones being able to play a major role in this. Thus it was crucial to be able to implement such characteristics. Second, this software was also chosen because it can deal with the effects of axonal arborescence on spike transmission and takes into account possible delays at branching nodes. For this, we assumed a standard set of electrophysiological values and Hodgkin and Huxley (HH) model ionic channel values that are characteristic of mammalian cortical axons. The latter were homogeneously distributed along morphology for all sections.

## Cortical synchrony and abnormal visual experience

As mentioned above, the reconstruction procedure induced a bias in the sampling of MD callosal axons toward those having larger diameters. However, most of the callosal connections between areas 17 and 18 have been reported as being mainly Y type (B or C), which have larger axonal diameters (23-27). Furthermore, these large myelinated axons are assumed to play a major role in precise spike timing and interhemispheric synchronization (64). In order to simulate the presence of myelin for propagation, we squared the diameters for sections which values were more than 0.28 micrometers, and we assigned them a low membrane capacitance value. This value was obtained from linear segment tests and thus reflects the well established experimental velocity value (cf. Results for detailed justifications). Results obtained with these assumptions indicate that the increased complexity of the architecture of the MD callosal axons does not induce any significant difference in the time distribution compared to normal structures. Of interest, this occurred in spite of the choice of 0.28 micrometers for the myelinated/non myelinated transition diameter: this provides the worst conditions for neural synchrony in the context of the present simulations (66).

The changes observed here in the morphology architecture of MD callosal axons compared to normals might have been accompanied by a significantly increase in the number of synapses per axon (including *en passant* ones) and/or an abnormal distribution of these synapses. This would have significantly increased the temporal dispersion of spike arrivals at the level of the callosal terminals of these axons. But surprisingly, this did not occur to any substantial degree. The number of terminal boutons did not increase significantly following monocular occlusion. In most cases, these boutons appeared as dense synaptic clusters situated near terminal ends as in normals (see axon BMO17-A3 in Figure 8 as an example). In addition, only few *en passant* synapses were actually present along the MD callosal terminals (unpublished data). This likely contributed to maintain temporal dispersion of spikes within the MD callosal terminals at values indistinguishable from NR group.

Concerning the impact of the morphology of the callosal axons on the spike timing distribution, our results confirm that, at least for myelinated fibers, the limited range of latencies of the transcallosal signals found here (~1-3 ms) is constrained by the high velocity imposed by myelination of axons. To investigate this as accurately as possible, careful attention was paid to the relation between axonal morphologies and biological plausibility. But the lack of information on ultra-structural parameters, in particular those related to precise myelin distribution and voltage-dependant channel distributions at nodes along mammalian visual callosal axons, forced us to exclude them from the compartmental model. Nevertheless our study shows that the homogeneous distribution (HH model) associated with the diameter squaring assumption are pertinent enough to provide a precise understanding of the spike timing distribution.

At branching nodes, experiments and models have shown that failure or delay in spike transmission may

occur. This depends mainly on a geometric ratio GR first introduced by Rall (cf. 91 for details), defined as a function of the diameters of the parent and daughter fibers. Similar to the callosal GR values reported by Innocenti and collaborators for NR cats, our estimation of callosal axon diameters in MD cats led to GR values lying between 0.5 and 2.0, a range in which failure almost never occurs (2-92-93). For this range of GR, each branching node could lead to an additional delay less than 0.1 ms (92-93-94). The procedure of diameter squaring, used to account for the presence of myelin sheaths, artificially increased the GR value by less than 0.5. We estimated that this may lead to an artificial additional delay inferior to 0.05 ms per bifurcation. Because less than six bifurcations are observed along the myelinated part of the MD callosal terminals, the total error due to the diameter squaring would not exceed 0.3 ms.

Compartmental models include the possibility of simulating effects of the myelin sheath on linear segments of axons using multi-layered modules, and mathematical models have studied the effect of myelin on branching points (60-62). However, the combination of both on complex axonal trees has not yet been implemented. Although, it has been shown that there is no myelin at branching nodes, a major difficulty is to adopt generic rules for placement of myelinated segments (lengths and Ranvier node positions) on axonal branches with variable lengths and diameters (59). Moreover, in our reconstructed axons, we do not have access to information permitting description of such ultra-structural parameters of myelin. In order to obtain such information, some intensive double-marking immunochemical techniques would need to be used. This would be particularly relevant for establishing on rules permitting to set myelin appropriately.

### 5.3. Possible role of synchronized activities in the development of callosal connections after early monocular deprivation

As a general rule, the characteristics of the temporal coding by neurons during development are not yet fully understood. Nevertheless, spike timing and synchronized activities play an important role both during fetal and postnatal life (e.g., for examples 95-96-97-98-99; cf. also 100-101 for reviews). This applies to visual callosal connections, whether they develop during normal or abnormal postnatal visual experience. Here, we have demonstrated that the dispersion of arrival times of spikes at the level of callosal terminals is preserved in cat visual cortex in spite of abnormalities in their architectures due to early MD. This may help to solve the above mentioned problem.

From electrophysiological data obtained from exploring cat visual cortex from 12 postnatal days to adulthood, it is known that callosal terminals in NR animals mostly activate visual cortical cells with receptive fields which are located in the central part of the visual field, either in the central vertical meridian or within the hemifield ipsilateral to the explored cortex (e.g. 23-25). Briefly, these data and others led authors to conclude that both the central vertical part of the retina (including the

## Cortical synchrony and abnormal visual experience

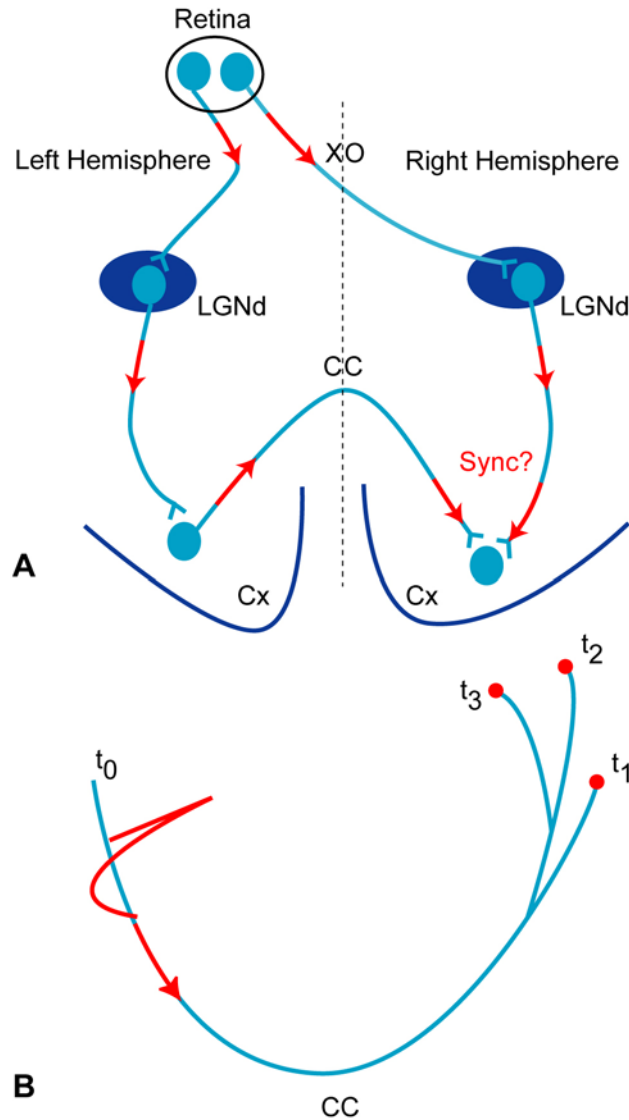


**Figure 10.** Two ways to achieve synchronized activity in the primary visual cortex while engaging the corpus callosum. A. The *unocular synchronization hypothesis*. Spiking activities are initiated from two adjacent ganglion cells in the retina (likely the central or the temporal one) of one eye and follow separate routes through two different visual pathways namely the crossed vs. uncrossed retino-geniculo-cortical ones. But, at the end, such activities converge in synchrony upon the same cortical locus within the contralateral hemisphere. B. *The small dispersion hypothesis*. A spike is initiated from one given visual cortical neuron in one hemisphere and reaches the other hemisphere only though the corpus callosum. It may reach the terminal axonal branches of this neuron within a short time window.

area centralis) and the temporal retina of the eye contralateral to the explored cortex are mainly implicated in activating these connections (e.g. 23-102). Based on these functional data as well as anatomical studies describing specific links between callosal connections and ocular dominance columns, Olavarria proposed the “unocular hypothesis” as the main mechanism to stabilize callosal linkages during normal development (102; cf. Figure 10A). This hypothesis suggests that correlated activities within visual cortex on one side may be driven by bilateral projections from both the central and the temporal retina of the contralateral eye. The first projection would be achieved by implicating the “uncrossing” retino-

geniculo-cortical pathway and the CC, while the second one would be achieved through the “crossing” retino-geniculo-cortical pathway only. This is possible because: (i) each eye in higher mammals sends axons to both hemispheres, with the temporal retina projecting mainly ipsilaterally and the nasal one projecting mainly contralaterally; (ii) some ganglion cells in the central part of the retina, namely the naso-temporal division, send their axons bilaterally (e.g. 103-104-105-106-107-108-109-110); (iii) some ganglion cells (5 to 10%) in the temporal retina project to the contralateral dorsal lateral geniculate nucleus (dLGN; e.g. 107-108-109-110-111-112-113).

## Cortical synchrony and abnormal visual experience

While the “unocular hypothesis” was proposed as a possible mechanism to stabilize callosal linkages during *normal* development, we propose here that it may also be implicated in abnormal conditions. This may be even more powerful in MD animals than in NR ones. This is because: (i) during the developmental period, MD animals have not any binocular competition (cf. 114 for further details); (ii) in such limited viewing conditions, some exuberant ganglion cell projections that are normally eliminated during development may be spared and stabilized in the adult. For example, it has been shown that more ganglion cells within the temporal retina project to the contralateral dLGN in adults whose optic tract has been sectioned early in life (e.g. 113-115-116); (iii) both callosal and geniculate-cortical terminals within the visual cortex ipsilateral to the occluded eye (as investigated here) have abnormalities in their architecture (cf. Results; e.g. also 117-118-119). Still they may interact properly one with the other since we demonstrate here that normal synchrony of neural activity may be preserved in spite of such abnormalities. The small temporal dispersion window reported here (regardless of the complexity of the axons) would thus help to synchronize the arrival of spikes along the two routes involved here (see Figure 10B, “small dispersion hypothesis”). Altogether, this “unocular” process may contribute actively to the selection of axons, of axonal branches and to the stabilization of synapses. Spikes at each individual callosal terminal arriving in synchrony with those conveyed through the “crossing” retino-geniculate-cortical fiber would contribute to such processes. This would be favored by the fact that both the retino-thalamic pathway and the thalamo-cortical one in MD cats undergo anatomical changes that are similar to those reported in the callosal pathway (117-118-119).

Another important issue is that the time of propagation of spikes along the callosal axons in the adult mammal is heavily dependent on the degree of myelination of axons. The fibers in the splenium of the CC are myelinated only during the second postnatal month in cats, i.e. rather late during the critical period (50-120). The majority of myelinated fibers in all cortical layers of the visual cortex also appears after the second postnatal month (121). More generally, most of the thalamo-cortical, cortico-cortical, intra- and inter-hemispheric connectivity develop without myelin. This indicates that most of the network that constitutes the visual system (including axons and synapses) is elaborated during the earliest phase of the critical period, when are only slow propagation of spikes may occur (e.g. 122) and when events less precisely temporally correlate (e.g. 123-124). Moreover, at this early stage of development, the architectures of the callosal axons are less complex than in adults because their development is not yet finished (125). Thus, in those conditions and without myelin, although our work does not apply directly, we suggest that synchronization still plays a role in the developing network at a slower time scale, with however small time dispersion.

### 5.4. Role of synchronized callosal activities during visual processing

As evoked in the Introduction, various studies have reported the emergence of gamma oscillations and

their synchronization both within and between hemispheres while functionally related regions of visual cortex are co-activated (28-30-31-32). The “perceptive binding by synchronization” hypothesis holds that perception become coherent via such synchronized activities (3-126). If the callosal circuits in MD animals do contribute to sustain intra- and interhemispheric synchronizations as well as to elaborate coherent perception, the dispersion of the transcallosal signals might be small enough to establish and maintain stable constructive oscillations locked in phase. This provided another reason to test the “small dispersion hypothesis” (cf. Figure 10B). Indeed, a low dispersion of the signal is a key parameter to establish and maintain stable oscillations. In the gamma frequency band, a dispersion of a few milliseconds is compatible with oscillations within this frequency range. The 3 ms dispersion reported here is precisely within the time window appropriate for establishing a functional callosal connection within a 8 ms duration, which is compatible with the 25 ms period for gamma oscillations at 40 Hz as described by Konig and collaborators (127). Altogether, our study thus suggests that callosal axons in MD animals are functionally capable of support any localized gamma synchronizations, which are expected to be implicated in visual perception.

## 6. ACKNOWLEDGMENTS

The authors thank Suzette Doutremer for skilful help with histological processing; Nicole Quenech’Du for the 3D-reconstructions; Nicolas Lebas for statistical analysis of the data, Murielle Bourge for animal care; France Maloumian for assistance in preparing of the figures. We also thank Dr. S. Wiener for useful comments on the manuscript as well as European Journal of Neuroscience and Wiley-Blackwell publisher for permitting reproducing figures 2, 4, 5, 11, 12, 13 from ref 1. This work was supported by the MENSER (ACI “Neurosciences Integratives et Computationnelles” to C. Milleret and ACI “Nouvelles interfaces avec les Mathématiques” to B. Teissier).

## 7. REFERENCES

1. Houzel JC, C Milleret, GM Innocenti: Morphology of callosal axons interconnecting areas 17 and 18 of the cat. *Eur J Neurosci* 6, 898-917 (1994)
2. Innocenti GM, P Lehmann, JC Houzel: Computational structure of visual callosal axons. *Eur J Neurosci* 6, 918-935 (1994)
3. Von Der Malsburg C. The correlation theory of brain function. In: Internal Report 81–82, Max Planck Institute, 1981. Reprinted in : Models of Neural Networks II. Eds: E Domany, JL van Hemmen, K Schulten. Springer, Berlin, 95-119 (1994)
4. Shadlen MN, JA Movshon: Synchrony unbound: a critical evaluation of the temporal binding hypothesis. *Neuron* 24, 67-77 (1999)

## Cortical synchrony and abnormal visual experience

5. Gray CM, W Singer: Stimulus-specific neuronal oscillations in orientation columns of cat visual cortex. *Proc Natl Acad Sci USA* 86, 1698-1702 (1989)
6. Gray CM, P Konig, AK Engel, W Singer: Oscillatory responses in cat visual cortex exhibit inter-columnar synchronization which reflects global stimulus properties. *Nature* 338, 334-337 (1989)
7. Nelson JI, PA Salin, MHJ Munk, M Arzi, J Bullier: Spatial and temporal coherence in cortico-cortical connections: a cross-correlation study in areas 17 and 18 in the cat. *Vis Neurosci* 9, 21-37 (1992)
8. Molotchnikoff S, S Shumikhina, LE Moisan: Stimulus-dependent oscillations in the cat visual cortex: differences between bar and grating stimuli. *Brain Res* 731, 91-100 (1996)
9. Roelfsema PR, VA Lamme, H Spekreijse: Synchrony and covariation of firing rates in the primary visual cortex during contour grouping. *Nat Neurosci* 7, 982-991 (2004)
10. Womelsdorf T, P Fries, PP Mitra, R Desimone: Gamma-band synchronization in visual cortex predicts speed of change detection. *Nature* 439, 733-736 (2006)
11. Fries P, T Womelsdorf, R Oostenveld, R Desimone: The effects of visual stimulation and selective visual attention on rhythmic neuronal synchronization in macaque area V4. *J Neurosci* 28, 4823-4835 (2008)
12. Ghisovan N, A Nemri, S Shumikhina, S Molotchnikoff: Synchrony between orientation-selective neurons is modulated during adaptation-induced plasticity in cat visual cortex. *BMC Neurosci* 3, 9-60 (2008)
13. Singer W. Response synchronization, gamma oscillations, and perceptual binding in cat primary visual cortex. In: The cat primary visual cortex. Eds: BR Payne, A Peters, Academic Press, A division of Harcourt Inc., San Diego, London, USA, 521-559 (2002)
14. Engel AK, P Konig, AK Kreiter, TB Schillen, W Singer: Temporal coding in the visual cortex: new vistas on integration in the nervous system. *Trends Neurosci* 15, 218-226 (1992)
15. Tallon-Baudry C, O Bertrand, C Delpuech, J Pernier: Oscillatory gamma-band (30-70 Hz) activity induced by a visual search task in humans. *J Neurosci* 17, 722-734 (1997)
16. Tallon-Baudry C, O Bertrand, F Peronnet, J Pernier: Induced gamma-band activity during the delay of a visual short-term memory task in humans. *J Neurosci* 18, 4244-4254 (1998)
17. Olavarria JF: Non-mirror symmetric patterns of callosal linkages in area 17 and 18 in cat visual cortex. *J Comp Neurol* 366, 643-655 (1996)
18. Innocenti GM: Postnatal development of corticocortical connections. *Ital J Neurol Sci (Suppl)* 5, 25-28 (1986)
19. Payne BR, DF Siwek: Visual-field map in the callosal recipient zone at the border between areas 17 and 18 in the cat. *Vis Neurosci* 7, 221-236 (1991)
20. Hubel DH, TN Wiesel: Cortical and callosal connections concerned with the vertical meridian of visual fields in the cat. *J Neurophysiol* 30, 1561-1573 (1967)
21. Berlucchi G, MS Gazzaniga, G Rizzolatti: Microelectrode analysis of transfer of visual information by the corpus callosum. *Arch Ital Biol* 105, 583-596 (1967)
22. Lepore F, JP Guillemot: Visual receptive field properties of cells innervated through the corpus callosum in the cat. *Exp Brain Res* 46, 413-424 (1982)
23. Payne BR: Function of the corpus callosum in the representation of the visual field in cat visual cortex. *Vis Neurosci* 5, 205-211 (1990)
24. Milleret C, P Buser: Reorganization processes in the visual cortex also depend on visual experience in the adult cat. *Prog Brain Res* 95, 257-269 (1993)
25. Milleret C, JC Houzel, P Buser: Pattern of development of the callosal transfer of visual information to cortical areas 17 and 18 in the cat. *Eur J Neurosci* 6, 193-202 (1994)
26. Innocenti GM: The primary visual pathway through the corpus callosum: morphological and functional aspects in the cat. *Arch Ital Biol* 118, 124-188 (1980)
27. McCourt ME, J Thalluri, GH Henry: Properties of area 17/18 border neurons contributing to the visual transcallosal pathway in the cat. *Vis Neurosci* 5, 83-98 (1990)
28. Engel AK, P Konig, AK Kreiter, W Singer: Interhemispheric synchronization of oscillatory neuronal responses in cat visual cortex. *Science* 252, 1177-1179 (1991)
29. Nowak LG, MH Munk, JI Nelson, AC James, J Bullier: Structural basis of cortical synchronization. I. Three types of interhemispheric coupling. *J Neurophysiol* 74, 2379-2400 (1995)
30. Kiper DC, MG Knyazeva, L Tettoni, GM Innocenti: Visual stimulus-dependent changes in interhemispheric EEG coherence in ferrets. *J Neurophysiol* 82, 3082-3094 (1999)
31. Knyazeva MG, DC Kiper, VY Vildavski, PA Despland, M Maeder-Ingvar, GM Innocenti: Visual stimulus-dependent changes in interhemispheric EEG coherence in humans. *J Neurophysiol* 82, 3095-3107 (1999)

## Cortical synchrony and abnormal visual experience

32. Carmeli C, L. Lopez-Aguado, KE Schmidt, O De Feo, GM Innocenti: A novel interhemispheric interaction: modulation of neural cooperativity in the visual areas. *PLoS One* 2, e1287 (2007)
33. Rochefort NL, P Buzas, N Quenech'Du, A Koza, UT Eysel, C Milleret, Z. Kisvarday: Functional selectivity of interhemispheric connections in cat visual cortex. *Cerebral Cortex* (in press)
34. Innocenti GM, DO Frost: Effects of visual experience on the maturation of the efferent system to the corpus callosum. *Nature* 280, 231-234 (1979)
35. Yinon U, A Hammer: Post-critical period plasticity of callosal transfer to visual cortex cells of cats following early conditioning of monocular deprivation and late optic chiasm transection. *Brain Res* 516, 84-90 (1990)
36. Milleret C, JC Houzel: Visual interhemispheric transfer to areas 17 and 18 in cats with convergent strabismus. *Eur J Neurosci* 13, 137-152 (2001)
37. Konig P, AK Engel, S Lowel, W Singer: Squint affects synchronization of oscillatory responses in cat visual cortex. *Eur J Neurosci* 5, 501-508 (1993)
38. Schmidt KF, S Lowel: Strabismus modifies intrinsic and inter-areal connections in cat area 18. *Neuroscience* 152, 128-137 (2008)
39. Ruthazer ES, CJ Akerman, HT Cline: Control of axon branch dynamics by correlated activity *in vivo*. *Science* 301, 66-70 (2003)
40. Ruthazer ES, HT Cline: Insights into activity-dependent map formation from the retinotectal system: a middle-of-the-brain perspective. *J Neurobiol* 59, 134-146 (2004)
41. Uesaka N, S Hirai, T Maruyama, ES Ruthazer, N Yamamoto: Activity dependence of cortical axon branch formation: a morphological and electrophysiological study using organotypic slice cultures. *J Neurosci* 25, 1-9 (2005)
42. Uesaka N, ES Ruthazer, N Yamamoto: The role of neural activity in cortical axon branching. *Neuroscientist* 12, 102-106 (2006)
43. Bruno RM, TT Hahn, DJ Wallace, CP Kock, B Sakmann: Sensory experience alters specific branches of individual corticocortical axons during development. *J Neurosci* 29, 3172-3181 (2009)
44. Innocenti GM, L Fiore, R Caminiti: Exuberant projection into the corpus callosum from the visual cortex of newborn cat. *Neurosci Lett* 4, 237-242 (1977)
45. Glaser EM, M Tagamets, NT McMullen, H Van der Loos: The image-combining computer microscope--an interactive instrument for morphometry of the nervous system. *J Neurosci Methods*, 8, 17-32 (1983)
46. Glaser JR, EM Glaser: Neuron imaging with NeuroLucida--a PC-based system for image combining microscopy. *Comput Med Imaging Graph* 14, 307-317 (1990)
47. Tettoni L, P Lehmann, JC Houzel, GM Innocenti: Maxxim, software for the analysis of multiple axonal arbors and their simulated activation. *J. Neurosci Methods* 67, 1-9 (1996)
48. Brette R, M Rudolph, T Carnevale, M Hiles, D Beeman, JM Bower, M Diesmann, A Morrison, PH Goodman, FC Harris Jr, M Zirpe, T Natschlag, D Pecevski, B Ermentrout, M Djurfeldt, A Lansner, O Rochel, T Vieville, E Muller, AP Davison, S El Boustami, A Destexhe: Simulation of networks of spiking neurons: a review of tools and strategies. *J Comput Neurosci* 23, 349-398 (2007)
49. Looney GA, AJ Elberger: Myelination of the corpus callosum in the cat: time course, topography, and functional implications. *J Comp Neurol* 248, 336-347 (1986)
50. Berbel P, GM Innocenti: The development of the corpus callosum in cats: a light- and electron-microscopic study. *J Comp Neurol* 276, 132-156 (1988)
51. Winfield DA: The postnatal development of synapses in the different laminae of the visual cortex in the normal kitten and in kittens with eyelid suture. *Brain Res* 285, 155-169 (1983)
52. Lyckman AW, S Horng, CA Leamey, D Tropea, A Watakabe, A Van Wart, C McCurry, T Yamamori, M Sur: Gene expression patterns in visual cortex during the critical period: synaptic stabilization and reversal by visual deprivation. *Proc Natl Acad Sci USA* 105, 9409-9414 (2008)
53. Rochefort N, N Quenech'du, L Watroba, M Mallat, C Giaume, C Milleret. Microglia and astrocytes may participate in the shaping of visual callosal projections during postnatal development. *J Physiol Paris* 96, 183-192 (2002)
54. Rochefort N, N Quenech' Du, P Ezan, C Giaume, C Milleret: Postnatal development of GFAP, connexins 43 and connexins 30 in cat visual cortex. *Brain Res Dev Brain Res* 160, 252-264 (2005)
55. O'Kusky J, M. Colonnier: Postnatal changes in the number of neurons and synapses in the visual cortex (area 17) of the macaque monkey: a stereological analysis in normal and monocularly deprived animals. *J Comp Neurol* 210, 291-306 (1982)
56. Hille B. Ion Channels of Excitable Membranes, third edition, Sinauer Associates, 2001
57. Peres A, F. Andrietti: Computer reconstruction of the spread of excitation in nerve terminals with inhomogeneous channel distribution. *Eur Biophys J* 13, 235-243 (1986)

## Cortical synchrony and abnormal visual experience

58. Rasband MN, P Shrager: Ion channel sequestration in central nervous system axons. *J Physiol* 525, 63-73 (2000)
59. Deschênes M, P Landry: Axonal branch diameter and spacing of nodes in the terminal arborization of identified thalamic and cortical neurons. *Brain Res* 191, 538-544 (1980)
60. Zhou L, SY Chiu: Computer model for action potential propagation through branch point in myelinated nerves. *J Neurophysiol* 85, 197-210 (2001)
61. Blight AR: Computer simulation of action potentials and afterpotentials in mammalian myelinated axons: the case for a lower resistance myelin sheath. *Neuroscience* 15, 13-31 (1985)
62. Halter JA, JW Jr Clark: A distributed-parameter model of the myelinated nerve fiber. *J Theor Biol* 148, 345-382 (1991)
63. McIntyre CC, AG Richardson, WM Grill: Modeling the excitability of mammalian nerve fibers: influence of afterpotentials on the recovery cycle. *J Neurophysiol* 87, 995-1006 (2002)
64. Wang SS, JR Shultz, MJ Burish, KH Harrison, PR Hof, LC Towns, MW Wagers, KD Wyatt: Functional trade-offs in white matter axonal scaling. *J Neurosci* 28, 4047-4056 (2008)
65. Waxman SG, MV Bennett: Relative conduction velocities of small myelinated and non-myelinated fibres in the central nervous system. *Nat New Biol* 238, 217-219 (1972)
66. Waxman SG, L Bangalore. Myelin function and saltatory conduction. In: Neuroglia, 2<sup>nd</sup> Edition. Eds: H Kettenmann, BR Ranson, Oxford University Press, New York, Chapter 21 (2004)
67. Dayan P, LF Abbott. Theoretical Neuroscience: computational and mathematical modeling of neural systems. MIT, Press, Cambridge, Mass, London (2001)
68. Scott A. Neuroscience: a mathematical primer. Springer Verlag, New York Inc (2002)
69. Bell J. Excitability behaviour of myelinated axon models. In: Reaction-Diffusion equations. Eds: KJ Brown, JA Lacey, Oxford University Press, Oxford, England, 95-116 (1990)
70. Fitzhugh R: Computation of impulse initiation and saltatory conduction in a myelinated nerve fiber. *Biophys J* 2, 11-21 (1962)
71. Moore JW, RW Joyner, MH Brill, SD Waxman, M Najar-Joa: Simulations of conduction in uniform myelinated fibers. Relative sensitivity to changes in nodal and internodal parameters. *Biophys J* 21, 147-160 (1978)
72. Binczak S, S Jacquir, JM Bilbault, VB Kazantsev, VI Nekorkin: Experimental study of electrical FitzHugh-Nagumo neurons with modified excitability. *Neural Network* 19, 684-93 (2006)
73. Spruston N, D Johnston: Perforated patch-clamp analysis of the passive membrane properties of three classes of hippocampal neurons. *J Neurophysiol* 67, 508-529 (1992)
74. Johnston D, S Wu. Foundation of cellular neurophysiology. MIT Press, Cambridge, Massachusetts, 1995
75. Hollander M, DA Wolfe. Nonparametric Statistical Methods, John Wiley and Sons, New York, USA (1973)
76. Gibbons JD. Nonparametric Statistical Inference, 2nd edition, M Dekker, New York, USA (1985)
77. Berman NE, BR Payne: Alterations in connections of the corpus callosum following convergent and divergent strabismus. *Brain Res* 274, 201-212 (1983)
78. Elberger AJ, EL Smith, JM White: Spatial dissociation of visual inputs alters the origin of the corpus callosum. *Neurosci Lett* 35, 19-24 (1983)
79. Wree A, G Kulig, P Gutmann, K Zilles: Modification of callosal afferents of the primary visual cortex ipsilateral to the remaining eye in rats monocularly enucleated at different stages of ontogeny. *Cell Tissue Res* 242, 433-436 (1985)
80. Olavarria JF: Development of visual callosal connections in neonatally enucleated rats. *J Comp Neurol* 260, 321-348 (1987)
81. Murphy EH, AM Grigonis: Postnatal development of the visual corpus callosum: the influence of activity of the retinofugal projections. *Behav Brain Res* 30, 151-163 (1988)
82. Cynader M, F Lepore, JP Guillemot: Inter-hemispheric competition during postnatal development. *Nature* 290, 139-140 (1981)
83. Cusick CG, RD Lund: Modification of visual callosal projections in rats. *J Comp Neurol* 212, 385-398 (1982)
84. Toldi J, JR Wolff, UH Wiese: Functional consequences of modification of callosal connections by perinatal enucleation in rat visual cortex. *Neuroscience* 33, 517-524 (1989)
85. Katz LC, CJ Shatz: Synaptic activity and the construction of cortical circuits. *Science* 274, 1132-1138 (1996)
86. Innocenti GM, DO Frost, J. Illes: Maturation of visual callosal connections in visually deprived kittens: a challenging critical period. *J Neurosci* 5, 255-267 (1985)

## Cortical synchrony and abnormal visual experience

87. Boire D, R Morris, M Pfitz, F Lepore, DO Frost: Effects of neonatal splitting of the optic chiasm on the development of feline visual callosal connections. *Exp Brain Res* 104, 275-286 (1995)
88. Zufferey PD, F Jin, H Nakamura, L Tettoni, GM Innocenti: The role of pattern vision in the development of cortico-cortical connections. *Eur J Neurosci* 11, 2669-2688 (1999)
89. Alekseenko SV, SN Toporova, PY Shkorbatova: Neuronal connections of eye-dominance columns in the cat cerebral cortex after monocular deprivation. *Neurosci Behav Physiol* 38, 669-675 (2008)
90. Meyer MP, SJ Smith: Evidence from *in vivo* imaging that synaptogenesis guides the growth and branching of axonal arbors by two distinct mechanisms. *J Neurosci* 26, 3604-3614 (2006)
91. Debanne D: Information processing in the axon. *Nat Rev Neurosci* 5, 304-316 (2004)
92. Manor Y, J Gonczarowski, I Segev: Propagation of action potentials along complex axonal trees. Model and implementation. *Biophys J* 60, 1411-1423 (1991a)
93. Manor Y, C Koch, I Segev: Effect of geometrical irregularities on propagation delay in axonal trees. *Biophys J* 60, 1424-1437 (1991b)
94. Segev I, E Schneidman: Axons as computing devices: basic insights gained from models. *J Physiol Paris* 93, 263-270 (1999)
95. Antonini A, MP Stryker: Development of individual geniculocortical arbors in cat striate cortex and effects of binocular impulse blockage. *J Neurosci* 13, 3549-3573 (1993)
96. McCormick DA, F Trent, AS Ramoa: Postnatal development of synchronized network oscillations in the ferret dorsal lateral geniculate and perigeniculate nuclei. *J Neurosci* 15, 5739-5752 (1995)
97. Penn AA, PA Riquelme, MB Feller, CJ Shatz: Competition in retinogeniculate patterning driven by spontaneous activity. *Science* 279, 2108-2112 (1998)
98. Cang J, RC Renteria, M Kaneko, X Liu, DR Copenhagen, MP Stryker: Development of precise maps in visual cortex requires patterned spontaneous activity in the retina. *Neuron* 48, 797-809 (2005)
99. Warland DK, AD Huberman, LM Chalupa: Dynamics of spontaneous activity in the fetal macaque retina during development of retinogeniculate pathways. *J Neurosci* 26, 5190-5197 (2006)
100. Sengpiel F, PC Kind: The role of activity in development of the visual system. *Curr Biol* 12, R818-R826 (2002)
101. Price DJ, H Kennedy, C Dehay, L Zhou, M Mercier, Y Jossin, AM Goffinet, F Tissir, D Blakey, Z Molnar: The development of cortical connections. *Eur J Neurosci* 23, 910-920 (2006)
102. Olavarria JF: Callosal connections correlate preferentially with ipsilateral cortical domains in cat areas 17 and 18, and with contralateral domains in the 17/18 transition zone. *J Comp Neurol* 433, 441-457 (2001)
103. Stone J: The naso-temporal division of the cat's retina. *J Comp Neurol* 126, 585-599 (1966)
104. Stone J, Y Fukuda: The naso-temporal division of the cat's retina re-examined in terms of Y-, X- and W-cells. *J Comp Neurol* 155, 377-394 (1974)
105. Kirk DL, WR Levick, BG Cleland, H Wassle: Crossed and uncrossed representation of the visual field by brisk-sustained and brisk-transient cat retinal ganglion cells. *Vision Res* 16, 225-231 (1976a)
106. Kirk DL, WR Levick, BG Cleland: The crossed or uncrossed destination of axons of sluggish-concentric and non-concentric cat retinal ganglion cells, with an overall synthesis of the visual field representation. *Vision Res* 16, 233-236 (1976b)
107. Cooper ML, JD Pettigrew: The decussation of the retinothalamic pathway in the cat, with a note on the major meridians of the cat's eye. *J Comp Neurol* 187, 285-311 (1979)
108. Illing RB, H Wassle: The retinal projection to the thalamus in the cat: a quantitative investigation and a comparison with the retinotectal pathway. *J Comp Neurol* 202, 265-285 (1981)
109. Terao N, A Inatomi, T Maeda: Anatomical evidence for the overlapped distribution of ipsilaterally and contralaterally projecting ganglion cells to the lateral geniculate nucleus in the cat retina: a morphologic study with fluorescent tracers. *Invest Ophthalmol Vis Sci* 23, 796-798 (1982)
110. Tassinari G, M Bentivoglio, S Chen, D Campara: Overlapping ipsilateral and contralateral retinal projections to the lateral geniculate nucleus and superior colliculus in the cat: a retrograde triple labelling study. *Brain Res Bull* 43, 127-139 (1997)
111. Kinston WJ, MA Vadas, PO Bishop: Multiple projection of the visual field to the medial portion of the dorsal lateral geniculate nucleus and the adjacent nuclei of the thalamus of the cat. *J Comp Neurol* 136, 295-316 (1969)
112. Fukuda Y, J Stone: Retinal distribution and central projections of Y-, X- and W-cells of the cat's retina. *J Neurophysiol* 37, 749-772 (1974)
113. Leventhal AG, JD Schall, SJ Ault, JM Provis, DJ Vitek: Class-specific cell death shapes the distribution and pattern of central projection of cat retinal ganglion cells. *J Neurosci* 8, 2011-2027 (1988a)

## Cortical synchrony and abnormal visual experience

114. Stryker MP, A Antonini: Factors shaping the corpus callosum. *J Comp Neurol* 433, 437-440 (2001)

115. Williams RW, MJ Bastiani, B Lia, LM Chalupa: Growth cones, dying axons and developmental fluctuations in the fiber population of the cat's optic nerve. *J Comp Neurol* 246, 32-69 (1986)

116. Leventhal AG, JD Schall, SJ Ault: Extrinsic determinants of retinal ganglion cell structure in the cat. *J Neurosci* 8, 2028-2038 (1988b)

117. Friedlander MJ, LR Stanford: Effects of monocular deprivation on the distribution of cell types in the LGNd: a sampling study with fine-tipped micropipettes. *Exp Brain Res* 53, 451-461 (1984)

118. Friedlander MJ, KA Martin, D Wassenhove-McCarthy: Effects of monocular visual deprivation on geniculocortical innervation of area 18 in cat. *J Neurosci* 11, 3268-3288 (1991)

119. Kossel A, S Lowel, J Bolz: Relationships between dendritic fields and functional architecture in striate cortex of normal and visually deprived cats. *J Neurosci* 15, 3913-3926 (1995)

120. Looney GA, AJ Elberger: Myelination of the corpus callosum in the cat: time course, topography, and functional implications. *J Comp Neurol* 248, 336-347 (1986)

121. Sherman SM, PD Spear: Organization of visual pathways in normal and visually deprived cats. *Physiol Rev* 62, 738-855 (1982)

122. Tsumoto T, K Suda: Postnatal development of corticotectal neurons in the kitten striate cortex: an electrophysiological study. *Brain Res* 313, 29-38 (1983)

123. Moneta ME, W Singer: Critical period plasticity of kitten visual cortex is not associated with enhanced susceptibility to electrical kindling. *Brain Res* 395, 104-109 (1986)

124. Lestienne R, E Gary-Bobo, J Przybyslawski, P Saillour, M Imbert: Temporal correlations in modulated evoked responses in the visual cortical cells of the cat. *Biol Cybern* 62, 425-40 (1990)

125. Callaway EM, LC Katz: Emergence and refinement of clustered horizontal connections in cat striate cortex. *J Neurosci* 10, 1134-1153 (1990)

126. Singer W: Neuronal synchrony: A versatile code for the definition of relations? *Neuron* 24, 49-65 (1999)

127. Konig P, AK Engel, W Singer: Relation between oscillatory activity and long-range synchronization in cat visual cortex. *Proc Natl Acad Sci USA* 92, 290-294 (1995)

**Abbreviations:** MD, monocularly deprived; CC, corpus callosum; NR, normally-reared; A17, visual cortical area

17; A18, visual cortical area 18; TZ, transition zone between A17 and A18; dLGN dorsal lateral geniculate nucleus.

**Key Words:** Corpus callosum, Interhemispheric Connections, Three-Dimensional Reconstruction, Plasticity Of Callosal Terminals, Spike Propagation, Compartmental Model, Synchrony

**Send correspondence to:** Chantal Milleret, Laboratoire de Physiologie de la Perception et de l'Action, College-de-France, UMR CNRS 7152, 11 Place Marcelin Berthelot, 75005 Paris, France, Tel: 33-1-44-271398, Fax: 33-1-44-271403, E-mail: chantal.milleret@college-de-france.fr

<http://www.bioscience.org/current/vol15.htm>